INRIA

INSTITUT NATIONAL DE RECHERCHE EN INFORMATIQUE ET EN AUTOMATIQUE

# *Dense Fluid Flow Estimation*

Thomas Corpetti , Etienne Mémin , Patrick Pérez

**N˚4009**

Septembre 2000

THÈME 3


ISSN 0249-6399 ISRN INRIA/RR--4009--FR+ENG

# Dense Fluid Flow Estimation

Thomas Corpetti , Etienne Mémin * , Patrick Pérez †

Thème 3 — Interaction homme-machine,
images, données, connaissances
Projet Vista

Rapport de recherche n ° 4009 — Septembre 2000 — 35 pages

**Abstract:** In this paper we address the problem of estimating and analyzing the motion in image sequences showing fluid phenomenon. Due to the great deal of spatial and temporal distortions that luminance patterns exhibit in images of fluid, standard techniques from Computer Vision, originally designed for quasi-rigid motions with stable salient features, are not well adapted in this context. In that prospect, we investigate a dedicated energy-based motion estimator. The considered functional includes an original data model relying on the continuity equation of fluid mechanics. This new data model, which is specifically designed to be embedded in a multiresolution framework, is associated to an original div-curl type regularization. The optimization of the global energy function is solved within an efficient multigrid scheme. The performances of the resulting fluid flow estimator are demonstrated both on synthetic and real (meteorological) image sequences.

**Key-words:** Fluid motion, continuity equation, div-curl regularization, optical flow, robust estimation

*(Résumé : tsvp)*

* IRISA - Université de Rennes 1, {tcorpett,memin}@irisa.fr
† Microsoft Research Center, Cambridge, pperez@microsoft.com

Unité de recherche INRIA Rennes
IRISA, Campus universitaire de Beaulieu, 35042 RENNES Cedex (France)
Téléphone : 02 99 84 71 00 - International : +33 2 99 84 71 00
Télécopie : 02 99 84 71 71 - International : +33 2 99 84 71 71

# Estimation Dense du Mouvement Fluide

**Résumé :** Nous traitons dans cet article le problème de l'estimation et de l'analyse du mouvement dans le cas de séquences d'images représentant des phénomènes fluides. Dans ce contexte, la luminance des images fait parfois apparaître de fortes distorsions spatiales et temporelles, rendant délicate l'utilisation de techniques standard issues de la Vision par Ordinateur, originalement conçues pour des mouvements rigides et reposant sur une hypothèse d'invariance de la fonction de luminance. Dans cette étude, nous proposons un estimateur de mouvement modélisé au moyen d'une formulation énergétique et spécialement dédié à l'estimation de mouvement fluide. La fonctionnelle considérée est composée d'un terme d'attache aux données original issu de l'équation de continuité de la mécanique des fluides. Ce nouveau modèle de données, spécifié pour être aisément intégré dans un schéma multi-résolution, est associé à une régularisation de type "Div-Curl". L'optimisation de la fonction globale d'énergie est conduite à l'aide d'un schéma multi-grille. Les performances de cet estimateur sont expérimentalement démontrées sur des images synthétiques et réelles (météorologiques).

**Mots-clé :** Mouvement fluide, équation de continuité, régularisation Div-Curl, flot optique, estimation robuste

# 1 Introduction

In a number of domains conditioning our everyday life, the analysis of image sequences describing fluid phenomenon is of the highest importance. In evironmental sciences such as oceanography, meteorology and climatology, the analysis of different types of satellite image sequences allows to characterize the way the ocean or the atmosphere evolves. It authorizes for instance to detect and track characteristic features such as fish eggs, larvae, or polluting agents in oceanography [43]. In a similar way, such an analysis allows to extract, characterize, and track dynamical entities such as vortices in meteorological images[11, 30, 33]. The detection as soon as possible of violent and sudden critical situations [39], which generally involves spatio-temporal analysis of such images, is also of crucial importance for weather now-casters. Besides, estimated flow fields in weather satellite imagery constitute an established and important data source for numerical model of weather prediction [38]. In medical imaging, one might be interested in blood flow analysis [1, 16] or in the estimation of deformation fields[10, 44]. In the field of fluid mechanics, aero or hydro-dynamical experiments now routinely produce different kinds of video data whose analysis allows a better understanding of certain types of fluid flows. In this domain, the extraction and the classification of the critical points of the flow for a compact representation of the velocity field is also widely studied [19, 18, 17, 36].

In all these domains, cameras offer in a versatile and non intrusive way huge amount of spatio-temporal data, as opposed to *in situ* measurement techniques which are complex, expensive, and which in addition supply only sparse informations. The extraction of dense kinematic entities such as motion fields or particle trajectories, the measurement of differential characteristics of the motion such as the divergence or the vorticity of the flow, [46], provide concerned experts or numerical models with a great deal of valuable informations. Unfortunately, unlike dedicated probes which measure directly the physical quantities of interest, images provide them only indirectly: they have to be extracted from the luminance data recorded in the 2D image frame, which might be quite involved.

In addition, the analysis of motion in such sequences is particularly challenging due to the great deal of spatial and temporal distortions that luminance patterns exhibit in observed fluid phenomena. Standard techniques from Computer Vision, originally designed for quasi-rigid motions with stable salient features, are not well adapted in this context. The design of alternate approaches dedicated to fluid motion thus constitutes a widely open domain of research. Our work is a contribution in that direction.

In the Computer Vision field, numerous techniques are available to estimate the bidimensional vector field of apparent motion, usually known as optical-flow. The most accurate and generic – in term of image applications – estimators [7, 26, 32, 28] are based on Horn and Schunck model [25]. They consist in the minimization of an energy functional composed of two terms: a data model term usually based on the *brightness conservation* assumption, and a regularization (or smoothness) term, capturing a *contextual regularity prior*. Although such standard methods have demonstrated good performances in the context of deformable [23] and even fluid motions [3, 11, 29], it remains that both assumptions are very likely not to hold in large areas of this images, due to the tridimensional and highly deformable nature

of fluid motions. The brightness assumption for instance does not hold in regions where the fluid exhibits 3D motions not parallel to the image plane. In such regions, usually characterized by a significant divergence of the apparent 2D motion field, the luminance function often undergoes large variations which account for fluctuation of matter density. This link between luminance and density is obvious in particle imaging. It is less straightforward in meteorological imaging. Nevertheless, the different channels used in that case (infra-red, water-vapor, or visible) are known to be related to fluid pressure or temperature, and as a consequence, undirectly to the matter density. Large variations of former physical quantities therefore imply image intensity variations, in contradiction with the brightness constancy assumption. In addition to this "brightness inconsistency", an optical-flow estimator equipped with a standard first-order regularization is unable to recover accurately the motion involved in such regions. Indeed, simple calculations [21] show that a first-order smoothness term favors laminar flow fields (low divergence and rotational everywhere), whereas one of these two differential quantities at least is usually significantly large in these areas of interest. Let us point out that a precise estimation of the motion within such areas is of the highest importance. As a matter of fact, these regions are the center of kinetics events such as vortices, sources or sinks which retain key information for describing, understanding and predicting the whole flow [18, 36, 33].

To cope with the two aforementioned problems, we propose here a dense motion estimator specifically dedicated to image sequences involving fluid phenomena. We first investigate a new data model which is not based on brightness conservation, but on the *continuity equation* of fluid mechanics. This idea originally suggested for motion estimation in [42] has already been considered in several studies since then. It has been used for instance in the context of fluid flows [14, 15, 44, 47] as well as in the context of medical imaging [44]. However, the continuity equation cannot be naturally embedded within standard incremental techniques of estimation. These hierarchical approaches, which resort to Gauss-Newton minimization are essential in case of large displacements [5, 13]. In order to use them in our context, we devise an integrated version of the continuity equation. Secondly, to deal with high concentrations of either divergence or vorticity, which are somewhat incompatible with the use of first-order regularization, we introduce a new "div-curl" regularization. This regularization departs from plain div-curl techniques introduced in [45, 22] by using an explicit estimation of the divergence and vorticity scalar fields.

This paper is organized as follows. In section II, we address the general problem of energy-based incremental estimation of optical-flow. We introduce the notations used throughout this paper and define a generic motion estimator which will be used as a basis for comparison purpose. In section III, we introduce the new data model based on the continuity equation of fluid flow. We then show that this constraint is somewhat incompatible with the use of first-order smoothness term. This observation leads us to propose, in section IV, an adapted smoothness term issuing from the ideas of div-curl regularization. The overall model and the associated optimization are detailed in section V. Comparative experimental results are reported and discussed in Section VI, and two examples of applications (reconstruction of trajectories and extraction of rotational/divergent structures) illustrate how the dense

vector fields provided by the new technique can be reliably used as an input for further computations of real practical interest.

## 2 Generic optical-flow estimator

Optical flow estimation aims at recovering the apparent displacement field $\boldsymbol{w} = \{\boldsymbol{w}(s), s \in S\}$ between two consecutive frames in an image sequence. Differential motion estimators are based on the so called optical-flow constraint equation (OFCE)[25]:

$$\boldsymbol{\nabla} f(s,t)^T \boldsymbol{w}(s) + f_t(s,t) = 0 \tag{1}$$

where $\boldsymbol{\nabla} f$ stands for the spatial gradient of the luminance function $f$ and $f_t(s,t) \triangleq f(s,t+1) - f(s,t)$ denotes the temporal luminance variation at location $s$. This equation issues from the linearization of the brightness constancy assumption $f(s+\boldsymbol{w}(s), t+1) - f(s,t) = 0$ with respect to unknown vector $\boldsymbol{w}(s)$.

It thus assumes that the unknown displacement remains in the domain of linearity of the luminance function. This hypothesis is particularly not verified for large displacements or around sharp edges. To circumvent these limitations an incremental approach based on a multiresolution image representation is often used [7, 13]. Such framework, involving a pyramidal decomposition of the image data [9], is unavoidable in numerous situations. In the following, we shall assume to work at a given resolution of such a pyramidal multiresolution structure. In the remain of the paper, the expressions and computations are thus meant to be reproduced at each resolution level according to a coarse-to-fine strategy.

Let us now suppose that a rough estimate $\boldsymbol{w} = \{\boldsymbol{w}(s), s \in S\}$ of the unknown velocity field is available from a previous estimation (e.g., from an estimation at lower resolution). Under the constant brightness assumption from time $t$ to $t+1$, a small *increment field* $\mathsf{d}\boldsymbol{w} \in \Omega \subset (\mathbb{R} \times \mathbb{R})^S$ can be estimated by minimizing the function $H \triangleq H_1 + \alpha H_2$, with [7, 31]:

$$H_1(\mathsf{d}\boldsymbol{w}) \triangleq \sum_{s \in S} \rho_1[\boldsymbol{\nabla} f(s+\boldsymbol{w}(s), t+1)^T \mathsf{d}\boldsymbol{w}(s) + f_t(s,t,\boldsymbol{w}(s))] \tag{2}$$

$$H_2(\mathsf{d}\boldsymbol{w}) \triangleq \sum_{<s,r> \in \mathcal{C}} \rho_2\left[\|(\boldsymbol{w}(s) + \mathsf{d}\boldsymbol{w}(s)) - (\boldsymbol{w}(r) + \mathsf{d}\boldsymbol{w}(r))\|\right] \tag{3}$$

where $f_t(s,t,\boldsymbol{w}(s)) \triangleq f(s+\boldsymbol{w}(s), t+1) - f(s,t)$, $\alpha > 0$ is a parameter balancing the two energy terms, $\mathcal{C}$ is the set of neighboring site pairs lying on grid $S$ equipped with some neighborhood system $\nu$ and functions $\rho_1$ and $\rho_2$ are standard *robust $M$-estimators* (with parameters $\sigma_1$ and $\sigma_2$). Functions $\rho_1$ and $\rho_2$ penalize respectively the *deviations* from the data model (i.e., the *displaced* OFCE ) and the departure from the smoothing prior.

Unlike quadratic penalty, these robust functions which are often non-convex for improved robustness [12] enable to limit the contribution of large residuals. Furthermore, assuming the concavity of $\phi(v) \triangleq \rho(\sqrt{v})$) [8, 20], the non-quadratic minimization of interest can be

turned conveniently into an augmented "semi-quadratic" one. Indeed, any multidimensional minimization problem of the form

$$\text{find} \arg\min_x \sum_i \phi[g_i^2(x)],$$

with $\phi$ concave, $\lim_{x\to\infty} \phi'(x) = 0$ and $\lim_{x\to 0^+} \phi'(x) = \tau < \infty$ can be turned into a dual minimization problem "find $\arg\min_{x,z} \sum_i [\tau z_i g_i^2(x) + \psi(z_i)]$" involving *auxiliary variables* (or *weights*) $z_i$'s continuously lying in $(0, 1]$, where $\psi$ is a continuously differentiable function depending on $\phi$.

The new associated minimization is then led *alternatively* with respect to $x$ and to the $z_i$'s. If $g_i$'s are affine, the augmented function is quadratic w.r.t. $x$, and the corresponding minimization leads to the resolution of a sparse linear system. Due to its huge dimension, iterative methods such as conjugate gradient, Gauss-Seidel or Jacobi methods are used to solve it. The principal unknown vector $x$ being frozen, the optimal weights are obtained in closed form [8, 20]:

$$\hat{z}_i(x) = \frac{\rho'[g_i(x)]}{2\tau g_i(x)} = \frac{1}{\tau}\phi'[g_i^2(x)]. \tag{4}$$

The whole alternate procedure constitutes an *iteratively reweighted least squares* estimation (IRLS) [24]. The convergence of this technique in a case where a non-convex robust estimator is involved, is investigated in [12]. In [34], the convergence of this algorithm has been further studied in the case where the convergence of the successive quadratic minimizations is not reached (which is the case in practice). It has been shown that, as long as the algorithm decreases the energy function (and provided that the iterates belong to a compact set), one only needs to perform few steps of an iterative solver between two successive weight updates. This results in a very efficient minimization: in the experiments reported in [34], the technique is about 5 times faster than standard IRLS for an image restoration, and about 3 times faster for optical flow estimation.

Let us now return to our problem. The weights under concern are of two natures: (a) *data outliers weights* (related to the dual formulation of $H_1$), and (b) *discontinuity weights* lying on the edge grid associated to $S$ (provided by the dual formulation of $H_2$). The first set of weights, denoted by $\delta = \{\delta_s, s \in S\}$, allows to attenuate the effect of data for which the OFCE is violated. The second one, denoted by $\beta = \{\beta_{sr}, <s,r> \in \mathcal{C}\}$, prevents from over-smoothing in locations exhibiting significant velocity discontinuities. The estimation is now expressed as the global minimization of the augmented semi-quadratic energy function $\mathcal{H} \triangleq \mathcal{H}_1 + \alpha\mathcal{H}_2$ where:

$$\mathcal{H}_1(\mathrm{d}\boldsymbol{w}) = \sum_{s\in S} \left[\tau_1 \delta_s \left[\boldsymbol{\nabla} f(s+\boldsymbol{w}(s), t+1)^T \mathrm{d}\boldsymbol{w}(s) + f_t(s,t,\boldsymbol{w}(s))\right]^2 + \psi_1(\delta_s)\right] \tag{5}$$

$$\mathcal{H}_2(\mathrm{d}\boldsymbol{w}) = \sum_{<s,r>\in\mathcal{C}} \left[\tau_2 \beta_{sr} \|(\boldsymbol{w}(s) + \mathrm{d}\boldsymbol{w}(s)) - (\boldsymbol{w}(r) + \mathrm{d}\boldsymbol{w}(r))\|^2 + \psi_2(\beta_{sr})\right]. \tag{6}$$

Note that this energy function can be seen as the discretization of the following functional:

$$\begin{aligned} J(\mathtt{d}\boldsymbol{w},\delta,\beta) = &\int_{\mathcal{S}} \tau_1 \delta(s) \left[\boldsymbol{\nabla}\tilde{f}(s)^T \mathtt{d}\boldsymbol{w}(s) + \tilde{f}_t(s)\right]^2 + \psi_1(\delta(s))\boldsymbol{ds} \\ &+ \alpha \int_{\mathcal{S}} \tau_2 \beta(s) \|\boldsymbol{\nabla}(\boldsymbol{w}(s) + \mathtt{d}\boldsymbol{w}(s))\|^2 + \psi_2(\beta(s))\boldsymbol{ds}, \end{aligned} \tag{7}$$

where $\boldsymbol{w}$ and $\mathtt{d}\boldsymbol{w}$ are, momentarily, two $C^1$-vector fields over continuous plane domain $\mathcal{S} \subset \mathbb{R}^2$, $\delta$ and $\beta$ two scalar fields on the same domain, and $\boldsymbol{\nabla}\tilde{f} \triangleq \boldsymbol{\nabla} f(. + \boldsymbol{w}, t+1)$, $\tilde{f}_t \triangleq f(. + \boldsymbol{w}, t+1) - f(., t)$.

As in the discrete step, the problem of minimizing this half-quadratic functional $J$ can be addressed in terms of alternate minimization [2, 27]. For fixed $\mathtt{d}\boldsymbol{w}$, Euler-Lagrange equations provide optimal expression of functions $\delta$ and $\beta$:

$$\delta = \frac{1}{\tau_1}\phi_1'[(\boldsymbol{\nabla}\tilde{f}^T\mathtt{d}\boldsymbol{w} + \tilde{f}_t)^2], \text{ and } \beta = \frac{1}{\tau_2}\phi_2'[\|\boldsymbol{\nabla}(\boldsymbol{w} + \mathtt{d}\boldsymbol{w})\|^2]. \tag{8}$$

The natural discretization of the first equation that consists in taking values of $\delta$, $\tilde{f}_t$, and $\boldsymbol{\nabla}\tilde{f}$ at pixel locations $\boldsymbol{s} = s \in S$, is readily obtained and yields exactly the same update rule as the one stemming from the minimization of discrete energy $\mathcal{H}$ w.r.t. $\{\delta_s\}_{s\in S}$. The same discretization scheme can be adopted for the second equation (as in [35]). However, if gradients are approximated by finite differences on the dual grid, it is simpler to have function $\beta$ discretized on the same edge lattice. The corresponding discretized update is then the same as the one that minimizes $\mathcal{H}$ w.r.t. $\{\beta_{sr}\}_{\langle s,t\rangle}$.

The weight functions $\delta$ and $\beta$ being fixed, one has to deal with the minimization of a quadratic functional of $\mathtt{d}\boldsymbol{w}$. This can be conducted first by writing down Euler-Lagrange equations as a necessary condition of optimality:

$$\tau_1\delta\boldsymbol{\nabla}\tilde{f}\boldsymbol{\nabla}\tilde{f}^T\mathtt{d}\boldsymbol{w} - \alpha\tau_2 \mathrm{div}[\beta\boldsymbol{\nabla}(\boldsymbol{w} + \mathtt{d}\boldsymbol{w})] = -\tau_1\delta\,\tilde{f}_t\boldsymbol{\nabla}\tilde{f}. \tag{9}$$

If $\boldsymbol{w}$, $\mathtt{d}\boldsymbol{w}$, and $\delta$ are discretized on $S$, while $\beta$, $\boldsymbol{\nabla}\boldsymbol{w}$, and $\boldsymbol{\nabla}\mathtt{d}\boldsymbol{w}$ are discretized on the dual grid, and the divergence operator is approximated by first-order central difference on $S$, this partial differential equation leads to a linear system that coincides with the one to be solved for minimizing $\mathcal{H}$ in $\mathtt{d}\boldsymbol{w}$.

We see that a standard discretization based on finite differences turns the minimization of continuous functional $J$ into the same problem as the one issuing from the minimization of discrete energy $\mathcal{H}$. Continuous formalism, however, allows more flexibility in the choice of discretization scheme since the discretization step is delayed: whereas discrete modeling sticks right away to the pixel grid discretization, variational approaches offer other choices, especially when finite element method is used (within Euler-Lagrange formalism [11], or apart from it [41]). In many cases, however, the discretization of the original continuous model is made as simple as possible w.r.t. pixel grid, thus yielding *in fine* the same discrete problems to be solved as those associated with the minimization of discrete energies.

The standard dense estimator defined as the minimization of $\mathcal{H}$ (or $J$) is general. It is only based on the assumptions of luminance conservation (first term) and of spatial smoothness of the motion (second term). It does not rely on any prior knowledge about typical fluid flows. This is the issue we turn to now.

# 3 Continuity equation

The optical-flow constraint equation has known limitations which can be partly circumvented. As already mentioned in the previous section, the influence of localized data-model deviations as those occurring in not too noisy situations or in small occlusion areas can be alleviated by the use of a robust cost function. In fluid imagery, the problem is much more complex. Image sequences representing fluid phenomena exhibit areas where the luminance function shows high temporal variations along the motion. These areas are often the center of tridimensional motions which cause the appearance or the disappearance of fluid matter within the bidimensional visualization plane. These regions are associated to divergent motions which influence greatly the shape of the velocity field in large surrounding areas. The estimation of the 2D apparent motion in that kind of regions is therefore of the highest importance and is hardly possible with the optical-flow constraint equation.

Instead of sticking to the intensity conservation assumption, we propose here to rely on the fluid conservation of mass law also known as *continuity equation*:

$$\frac{\partial \chi}{\partial t} + \mathrm{div}(\chi \mathbf{v}) = 0, \tag{10}$$

where $\chi$ denotes the density of the fluid, $\mathbf{v}$ its velocity and $\mathrm{div}\mathbf{v} = \frac{\partial u}{\partial x} + \frac{\partial v}{\partial y} + \frac{\partial w}{\partial z}$ stands for the divergence of the vector field $\mathbf{v} = (u, v, w)$. This 3D equation stems from the assumption that the temporal variation of mass within a given volume amounts to the mass flux entering this volume. Since

$$\mathrm{div}(\chi \mathbf{v}) = \boldsymbol{\nabla} \chi^T \mathbf{v} + \chi \mathrm{div}\mathbf{v}, \tag{11}$$

the equation of continuity may also be written

$$\frac{\partial \chi}{\partial t} + \boldsymbol{\nabla} \chi^T \mathbf{v} + \chi \mathrm{div}\mathbf{v} = 0. \tag{12}$$

Using the total derivative $\frac{d\chi}{dt} = \frac{\partial \chi}{\partial t} + \boldsymbol{\nabla} \chi^T \mathbf{v}$, this also reads:

$$\frac{d\chi}{dt} + \chi \mathrm{div}\mathbf{v} = 0. \tag{13}$$

Identifying the density with the luminance function one gets then exactly the optical-flow constraint equation (Eq.1) when the divergence of the 3D apparent flow vanishes. The continuity equation originally introduced in [14, 42] as a data model for motion estimation

of intensity time varying images has been since incorporated in several works. Surprisingly first applied to rigid body motion estimation [14, 42], it has been considered in the context of fluid imagery either for satellite meteorological images [4] or for experimental fluid mechanics [47]. It has also been introduced in medical imaging domain to recover 3D deformation fields of the heart [44] or to analyze blood flow [1, 16]. In all cases, this model has proven as an appealing alternative to standard luminance constancy assumption.

The use of continuity equation for image sequences analysis relies on the hypothesis that the image retains the main physical properties of the observed fluid. This critical hypothesis is twofold. First the luminance function is assumed to be somehow related to a passive quantity transported by the fluid. Secondly, the 2D representation of a fluid following a conservation law is assumed to respect a 2D continuity equation. This latter assumption has been theoretically verified in the case of transmittance imaging by Fitzpatrick [15] and extended in [47] for different border conditions. In the present work we will assume these two assumptions. This provides us with an alternative to the OFCE:

$$\frac{df}{dt} + f \mathrm{div} \boldsymbol{w} = 0. \tag{14}$$

However, a data model based on the continuity equation shares some limitations with one based on the optical-flow constraint equation. It is highly sensitive to the presence of noise and is very unlikely to hold everywhere. We then suggest to handle the continuity equation with a robust penalty function in our data model (in the same way as we did for the optical flow constraint in the generic model of estimation).

The other problem is that the continuity equation is related to fluid *velocity* and not to particle *displacements* [37]. Unlike brightness constancy $f(s + \boldsymbol{w}(s), t + 1) = f(s, t)$ which concerns displacements, it thus cannot be directly incorporated within an incremental multiresolution or multigrid framework. To cope with this problem, let us assume that the velocity field is stationary between the instants $t$ and $t + \Delta t$. The integration of the differential equation (14) from time $t$ to time $t + \Delta t$ yields a new expression of the intensity variation:

$$f(s + \Delta t \boldsymbol{w}(s), t + \Delta t) = f(s, t) \exp\Big( - \Delta t \ \mathrm{div} \ \boldsymbol{w}(s)\Big). \tag{15}$$

This equation can now serve as the basis constraint of a new fluid motion estimator. Setting $\Delta t = 1$ for notational convenience, a robust expression of the resulting data-model is:

$$\int_{\mathcal{S}} \rho\Big\{ f\left(s + \boldsymbol{w}(s), t + 1\right) \exp\left(\mathrm{div} \boldsymbol{w}(s)\right) - f(s, t) \Big\} d\boldsymbol{s}. \tag{16}$$

The term $\exp(\mathrm{div}\boldsymbol{w}(s))$ accounts for the intensity loss or gain exhibited by the fluid at locations where the motion is divergent. For example, in case of motion with positive divergence, there is a loss of intensity, which is all the more important than $\mathrm{div}\boldsymbol{w}(s)$ is large. We can note that if $\mathrm{div}\boldsymbol{w}(s) = 0$ (as in incompressible fluids), we end up with the brightness conservation assumption $f(s + \boldsymbol{w}(s), t + 1) - f(s, t)$ of standard optical flow techniques.

This integrated version of the continuity equation has the advantage to deal explicitly with displacements. An incremental form of this constraint may be readily obtained by a linearization of the weighted displaced luminance function
$f(s + \boldsymbol{w}(s) + \mathrm{d}\boldsymbol{w}(s), t+1) \exp(\mathrm{div}(\boldsymbol{w}(s) + \mathrm{d}\boldsymbol{w}(s)))$ around $\boldsymbol{w}(s)$. Dropping the time indices of the luminance function for sake of clarity, this linearization yields:

$$H_1(\mathrm{d}\boldsymbol{w}) = \int_{\mathcal{S}} \rho\Big\{ \exp(\mathrm{div}\boldsymbol{w}(s)) \left( \left[ \tilde{f}(s) \nabla \mathrm{div}\boldsymbol{w}(s) + \nabla \tilde{f}(s) \right]^T \mathrm{d}\boldsymbol{w}(s) + \tilde{f}(s) \right) - f(s) \Big\} d\boldsymbol{s}, \quad (17)$$

where $\tilde{f}(s) \triangleq f(s + \boldsymbol{w}(s), t+1)$.

We now turn to the definition of the smoothness prior to be used in conjunction with this new data energy term.

# 4 Adapted Div-Curl regularization

By using Euler-Lagrange conditions of optimality, it is readily demonstrated (see the appendix) that the standard first-order regularization functional

$$H_2(\boldsymbol{w}) = \alpha \int_{\mathcal{S}} (\|\boldsymbol{\nabla} u(s)\|^2 + \|\boldsymbol{\nabla} v(s)\|^2) d\boldsymbol{s},$$

is equivalent from the minimization point of view to a so-called *div-curl* regularization functional [45]:

$$H_2(\boldsymbol{w}) = \alpha \int_{\mathcal{S}} (\mathrm{div}^2 \boldsymbol{w}(s) + \mathrm{curl}^2 \boldsymbol{w}(s)) d\boldsymbol{s}, \quad (18)$$

where $\mathrm{div}\boldsymbol{w} = \frac{\partial u}{\partial x} + \frac{\partial v}{\partial y}$ and $\mathrm{curl}\boldsymbol{w} = \frac{\partial v}{\partial x} - \frac{\partial u}{\partial y}$ are respectively the divergence and the vorticity of the vector field $\boldsymbol{w} = (u, v)$.

A first-order regularization therefore penalizes the amplitude of both the divergence and the vorticity of the vector field. Consequently, it introduces concomitant constraints on the curl and divergence of the flow field. For fluid motion estimation, this does not seem appropriate since the apparent velocity field usually exhibits "concentrations" of vorticity and/or divergence corresponding to vortices or 3D motions non parallel to the image plane. In addition, an under-estimation of the divergence would be all the more prejudicial in our case, because the data model includes an explicit use of this quantity. Following the usual idea behind div-curl regularization [22] [45], which consists in decoupling the smoothing of each quantity, we propose here to introduce an adaptive div-curl smoothness that captures the physical prior we have on the different components of the Helmotz decomposition of the displacement field.

This representation decomposes the vector field $\boldsymbol{w}$ as a summation of three components (see Fig. 1): a smooth *laminar* field with $(\mathrm{div}\boldsymbol{w}, \mathrm{curl}\boldsymbol{w}) \equiv (0, 0)$, a divergence-free or

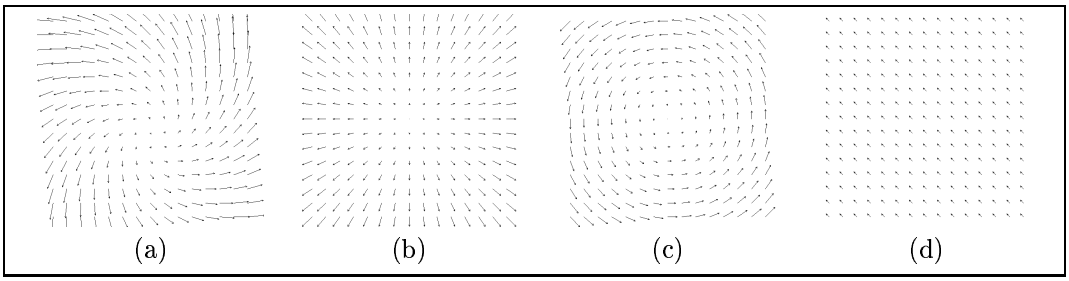


Figure 1: *Helmotz decomposition : (a) vector field; (b) divergence component; (c) vorticity component; (d) laminar component (a translation here)*

solenoidal component ($\mathrm{div}\boldsymbol{w} \equiv 0$) and a curl-free or irrotational component ($\mathrm{curl}\boldsymbol{w} \equiv 0$). Each of these components is equipped with its own prior: for solenoidal and irrotational fields it is a prior that allows substantial variations of the div and curl respectively, whereas a strong first-order regularization is used for the laminar component. To this end, we introduce the new smoothness term:

$$H_2(\boldsymbol{w}) \triangleq \alpha \int_{\mathcal{S}} \Big( \rho\left(\mathrm{div}\ \boldsymbol{w}(s) - \xi(s)\right) + \rho\left(\mathrm{curl}\ \boldsymbol{w}(s) - \zeta(s)\right) \Big) d\boldsymbol{s} + \lambda \int_{\mathcal{S}} \Big( \|\boldsymbol{\nabla}\xi(s)\|^2 + \|\boldsymbol{\nabla}\zeta(s)\|^2 \Big) d\boldsymbol{s}, \tag{19}$$

where scalars function $\xi$ and $\zeta$ are respectively some estimates of the divergence and the curl functions, and $\lambda$ is a positive parameter. This smoothness prior amounts to a first-order regularization when the estimates of the divergence and the vorticity both approach zero. At the opposite, when they are significantly non-null, a smoothing of the estimated divergence and curl of the flow field is imposed through the quadratic smoothness term. The first term enforces the vorticity and the divergence of the flow field to comply with their independent estimates. The robust penalty function $\rho$ used in these terms allows nevertheless the actual divergence and curl of the flow to depart significantly from the first-order smoothness prior undirectly put on them through $\xi$ and $\zeta$. This is important for recovering accurately the various concentrations of divergence and vorticity which are likely to be present. Getting ride of the auxiliary scalar fields $\xi$ and $\zeta$ in (19) (by setting $\xi = \mathrm{div}$ and $\zeta = \mathrm{curl}$) would amount to a standard second order div-curl regularization [45, 22]:

$$\int_{\mathcal{S}} \Big( \|\boldsymbol{\nabla}\mathrm{div}\boldsymbol{w}(s)\|^2 + \|\boldsymbol{\nabla}\mathrm{curl}\boldsymbol{w}(s)\|^2 \Big) d\boldsymbol{s}. \tag{20}$$

This however would not allow as easily as with our functional the specification of various robust priors on the divergence and the rotational. The second part of our functional (19) could indeed be easily modified to incorporate more drastic priors on these scalar fields such as those based on Rankine vortex model [33, 36]. Some physical measures provided by

dedicated probes, such as vorticity measurements obtained with hot wire anemometry [46] could also be easily imposed. By introducing new variables we avoid furthermore to handle the fourth-order coupled PDE's to which (20) leads [22].

# 5 Overall dedicated model

## 5.1 Discrete formulation

Gathering all the elements described so far, we can now write a global energy model for fluid motion estimation. As mentioned before, at this time one can choose either a continuous formulation and delay the discretization, or to discretize right away the energy functional. As in the case of the generic motion estimator, we chose the second solution. Given a previous estimate $\boldsymbol{w}$ to be refined, the estimation of an increment field $\mathrm{d}\boldsymbol{w}$ is formulated as the minimization of a global energy function composed of two terms $H \triangleq H_1 + H_2$ with

$$H_1(\mathrm{d}\boldsymbol{w}) \triangleq \sum_{s\in S} \rho_1\Big\{ \exp(\mathrm{div}\boldsymbol{w}(s)) \left( \left[ \tilde{f}(s)\nabla \mathrm{div}\boldsymbol{w}(s) + \nabla \tilde{f}(s) \right]^T \mathrm{d}\boldsymbol{w}(s) + \tilde{f}(s) \right) - f(s) \Big\} \quad (21)$$

and

$$\begin{aligned} H_2(\mathrm{d}\boldsymbol{w}, \xi, \zeta) \triangleq \alpha \sum_{s\in S} \Big( \rho_2 \left\{ \mathrm{div}(\boldsymbol{w} + \mathrm{d}\boldsymbol{w})(s) - \xi_s \right\} + \rho_2 \left\{ \mathrm{curl}(\boldsymbol{w} + \mathrm{d}\boldsymbol{w})(s) - \zeta_s \right\} \Big) \\ + \lambda \sum_{\langle s,r\rangle \in \mathcal{C}} \|\xi_s - \xi_r\|^2 + \|\zeta_s - \zeta_r\|^2, \end{aligned} \quad (22)$$

where $\mathcal{C}$ is the set of neighboring site pairs with respect to a first-order neighborhood system, and div $\boldsymbol{w}(s)$ (resp. curl$\boldsymbol{w}(s)$) denotes a discretization of the divergence (resp. the curl) of the vector field $\boldsymbol{w} = (u, v)$. Instead of using the standard central finite difference discretization scheme of such quantities

$$\begin{cases} \mathrm{div}\boldsymbol{w}(i,j) = \dfrac{1}{2}[(u_{i,j+1} - u_{i,j-1}) + (v_{i+1,j} - v_{i-1,j})], \\ \mathrm{curl}\boldsymbol{w}(i,j) = \dfrac{1}{2}[(v_{i,j+1} - v_{i,j-1}) - (u_{i+1,j} - u_{i-1,j})], \end{cases}$$

which does not include the central point $(i, j)$ – and consequently yields some difficulties in the resolution of associated equations –, we rather preferred to use a non-symmetric discretization of the partial derivatives including the current point at which the computation is carried out. This discretization scheme is given by:

$$\begin{cases} \mathrm{div}\boldsymbol{w}(i,j) = \dfrac{1}{6}[(3u_{i,j} + u_{i,j-2} - 6u_{i,j-1} + 2u_{i,j+1}) + (3v_{i,j} + v_{i-2,j} - 6v_{i-1,j} + 2v_{i+1,j})], \\ \mathrm{curl}\boldsymbol{w}(i,j) = \dfrac{1}{6}[(3v_{i,j} + v_{i,j-2} - 6v_{i,j-1} + 2v_{i,j+1}) - (3u_{i,j} + u_{i-2,j} - 6u_{i-1,j} + 2u_{i+1,j})]. \end{cases} \quad (23)$$

As for the minimization of the overall energy function, two main sets of variables have to be estimated. The first one is the incremental motion field $\mathsf{d}\boldsymbol{w}$, and the second one consists in the two scalar fields $\xi$ and $\zeta$. Following the same principle as for the generic estimator, the robust energy function is rewritten according to its half-quadratic formulation and minimized alternatively with respect to these two sets of variables and their associated weights until convergence. The weighted quadratic reformulation $\mathcal{H} \triangleq \mathcal{H}_1 + \alpha\mathcal{H}_2$ of $H$ is defined by:

$$\mathcal{H}_1(\mathsf{d}\boldsymbol{w}, \xi, \delta) \triangleq \sum_{s\in S} \tau_1 \delta_s \Big\{ \exp(\mathrm{div}\boldsymbol{w}(s)) \Big( \Big[ \tilde{f}(s) \nabla \mathrm{div}\boldsymbol{w}(s) + \nabla \tilde{f}(s) \Big]^T \mathsf{d}\boldsymbol{w}(s) + \tilde{f}(s) \Big) - f(s) \Big\}^2 + \psi_1(\delta_s), \tag{24}$$

and

$$\mathcal{H}_2(\mathsf{d}\boldsymbol{w}, \xi, \zeta, \varphi, \varsigma) \triangleq \sum_{s\in S} \tau_2 \varphi_s \Big( \mathrm{div}(\boldsymbol{w} + \mathsf{d}\boldsymbol{w})(s) - \xi_s \Big)^2 + \psi_2(\varphi_s) + \tau_2 \varsigma_s \Big( \mathrm{curl}(\boldsymbol{w} + \mathsf{d}\boldsymbol{w})(s) - \zeta_s \Big)^2 + \psi_2(\varsigma_s) + \lambda \sum_{\langle s,r\rangle \in \mathcal{C}} \|\xi_s - \xi_r\|^2 + \|\zeta_s - \zeta_r\|^2. \tag{25}$$

The different auxiliary variable fields $\delta$, $\varphi$ and $\varsigma$ weight respectively the data model, the curl-based prior term and the div-based prior term. Let us now see in details how are conducted the different minimizations constituting the overall alternated optimization process.

## 5.2 Minimization w.r.t. the increment motion field

Considering the div and curl estimates $\xi$ and $\zeta$ as being fixed, the minimization with respect to $\mathsf{d}\boldsymbol{w}$ amounts to solving a standard weighted least squares problem. This is conducted here with an efficient multi-parametric adaptive multigrid technique introduced in [32]. This scheme consists in solving the optimization problem as a cascade of constrained estimations. At a given level, $\ell$, of this hierarchical minimization the minimizer is constrained to be piecewise-parametric relatively to an image partition which becomes finer and finer as $\ell$ decreases. Each associated minimization is based on the rewriting of the global energy according to the considered constraint. Imposing at a given level, $\ell$, the increment field to be of the form $\mathsf{d}\boldsymbol{w}^\ell = \{P_n(s)\boldsymbol{\theta}_n^\ell, s \in B_n^\ell, n = 1, \cdots, N^\ell\}$, according to a block partition $\mathcal{B}^\ell = \{B_n^\ell, n = 1, \ldots, N^\ell\}$, where $P_n(s)$ is a matrix depending on the parameterization and $\boldsymbol{\theta}_n^\ell$ denotes the parameter vector for block $\mathcal{B}_n^\ell$ , we have $\mathcal{H}^\ell = \mathcal{H}_1^\ell + \alpha\mathcal{H}_2^\ell$ with:

$$\mathcal{H}_1^\ell(\mathsf{d}\boldsymbol{w}^\ell, \xi, \delta) = \sum_n \sum_{s\in B_n^\ell} \tau_1 \delta_s \Big\{ \exp(\mathrm{div}\boldsymbol{w}(s)) \Big( \Big[ \nabla \mathrm{div}\boldsymbol{w}(s) \tilde{f}(s) + \nabla \tilde{f}(s) \Big]^T P_n(s)\boldsymbol{\theta}_n^\ell + \tilde{f}(s) \Big) - f(s) \Big\}^2 + \psi_1(\delta_s) \tag{26}$$

and

$$\mathcal{H}_2^\ell(\mathtt{d}\boldsymbol{w}^\ell,\xi,\zeta,\varsigma,\varphi) = \alpha \sum_n \sum_{s\in B_n^\ell} \Big\{ \tau_2\varphi_s \Big(\mathrm{div}(\boldsymbol{w}+\mathtt{d}\boldsymbol{w}^\ell)(s) - \xi_s\Big)^2 + \psi_2(\varphi_s) + \tau_2\varsigma_s \Big(\mathrm{curl}(\boldsymbol{w}+\mathtt{d}\boldsymbol{w}^\ell)(s) - \zeta_s\Big)^2 + \psi_2(\varsigma_s)\Big\} + \lambda \sum_{\langle s,r\rangle\in\mathcal{C}} \|\xi_s-\xi_r\|^2 + \|\zeta_s-\zeta_r\|^2. \tag{27}$$

A particular attention must be paid to the expression of div $\mathtt{d}\boldsymbol{w}^\ell(s)$ and curl $\mathtt{d}\boldsymbol{w}^\ell(s)$ in this rewriting. Indeed, at each point where the support of discretized div and curl operators (Equ.23) straddles several blocks, computation involves a variable number of neighboring blocks. It must be noted that parameters $\boldsymbol{\theta}_n^\ell, n = 1,\cdots,N^\ell$ which define the constrained increments are locally inter-dependent in this non-regular way. At first levels, one has to face a reduced complexity half-quadratic minimization problem. As complexity increases with the decrease of $\ell$, the estimations provided by first levels are hopefully good enough to make the current minimization more tractable. At each level, we use an alternated minimization. The semi-quadratic energy is processed through one or few steps of an adequate iterative solver, which guarantees an energy decrease, and then weights $\delta$, $\varphi$ and $\varsigma$ are updated according to (4). The hierarchy of levels is generated by splitting a crude original partition. All the levels are visited in a coarse-to-fine strategy. At the end of each grid level, in the same spirit as Gauss-Newton minimization, the estimate $\mathtt{d}\hat{\boldsymbol{w}}^\ell$ is integrated in the whole displacement field ($\boldsymbol{w} \leftarrow \boldsymbol{w} + \mathtt{d}\hat{\boldsymbol{w}}^\ell$). This implies in particular that the displaced luminance function $\tilde{f}$ is recomputed to account for the additional displacement $\mathtt{d}\hat{\boldsymbol{w}}^\ell$. The increment field at each level as well as the field to be refined $\boldsymbol{w}$ is initialized with a null field.

The block partition supporting the constrained increments may be adaptive or regular and different parameterizations may be used simultaneously or successively [32]. In this work, we used a regular block partition associated to a piecewise 6-parameter affine constraint ($P_n(s=(x_s,y_s)) = \begin{bmatrix}1 & x_s & y_s & 0 & 0 & 0\\ 0 & 0 & 0 & 1 & x_s & y_s\end{bmatrix}$, $\boldsymbol{\theta}_n^\ell \in \mathbb{R}^6$) for blocks bigger than 4 sites, whereas a translational constraint ($\boldsymbol{\theta}_n^\ell = \mathtt{d}\boldsymbol{w}^\ell \in \mathbb{R}^2$) is imposed for smaller blocks.

## 5.3 Minimization w.r.t. the div and curl scalar fields

Considering in turn, the motion field and its related auxiliary variable fields as being frozen, we now have to perform an alternated minimization according to the divergence and curl scalar fields $\xi$ and $\zeta$. Both minimizations are exactly of the same nature, we therefore present only the minimization w.r.t. the $\zeta$ variables.

The energy terms involved in this minimization are:

$$\sum_{s\in S} \Big\{ \tau_2\varsigma_s \Big(\mathrm{curl}(\boldsymbol{w}+\mathtt{d}\boldsymbol{w}^\ell)(s) - \zeta_s\Big)^2 + \psi_2(\varsigma_s)\Big\} + \frac{\lambda}{\alpha} \sum_{\langle s,r\rangle\in\mathcal{C}} \|\zeta_s-\zeta_r\|^2. \tag{28}$$

We have here to solve a half-quadratic problem. At fixed weights the energy descent is performed using one step of Gauss-Seidel iterative solver. The weights are then updated according to (4).

# 6 Experimental results

In this section we present a variety of experimental results. In order to assess the performances of the proposed dedicated approach, we have systematically compared the obtained motion fields to those estimated with the generic robust technique. In both cases, we choose the Leclerc estimator $\rho(x) = 1 - \exp(-\tau x^2)$, both for the data term and for the smoothness term. As for the parameters, it is important to point out that those in common have been tuned to exactly the same values. Besides, these values have been kept unchanged for all the experiments (see table 1).

Table 1: parameter values

| $\alpha$ | $\lambda$ | $\tau_1$ | $\tau_2$ | #grid levels | #resolution levels |
|---|---|---|---|---|---|
| 50 | 10 | 2.7 | 1.0 | 4 | 3 |

In order to evaluate quantitatively the results of the dedicated fluid flow motion estimator we first carried out experiences on synthetic sequences.

## 6.1 Synthetics results

The two motion estimation techniques (generic and dedicated ones) have been applied and compared on four synthetic sequences built by applying a known motion to a real Meteosat image. The three first examples are depicted in figure 2. They are respectively characterized by a synthetic diverging motion (Fig. 2b), a rotational motion (Fig. 2c), and a swirling motion (Fig. 2d). The value of the divergence and curl applied are given in table 2. These synthetic sequences have been chosen to evaluate the benefit of the new div-curl regularization term. We list in table 2 the average divergence and vorticity estimated respectively with the robust first-order regularization (6) and with the robust adapted div-curl one (22). Furthermore, to assess also the usefulness of the robust penalty term in the adapted div-curl regularization, we give the results provided by a quadratic version of this smoothness term. These three kinds of regularization have been associated here to the same robust data model based on the optical flow constraint equation from which the synthetic second image is derived. Quantitative comparative results are gathered in table 2. The mean square error is defined as follows:

$$MSE = \frac{\sqrt{\sum_{s \in S} \left( f(s,t) - \tilde{f}(s) \right)^2}}{\mid S \mid},$$

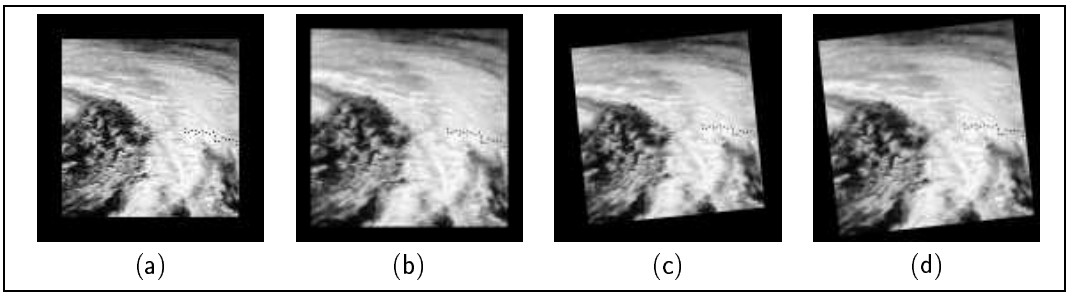


Figure 2: *(a) Real Meteosat image (visible channel); (b) result of a synthetic divergence ($div = 0.2$); (c) result of a synthetic rotation ($curl = -0.2$); (d) result of a synthetic swirl ($(div, curl) = (0.2, -0.2)$)*

where $\tilde{f}(s) = f(s+\boldsymbol{w}(s), t+1)$ is the reconstructed image obtained by applying the estimated motion field to the second image, ans $\mid S \mid$ is the image size. This quantitative measure is an indicator about the quality of the estimated motion field *under the assumption of brightness constancy*. For these synthetic examples built on that assumption, it is then a relevant evaluation criterion. We also report the average div and curl, computed as $\frac{\sum_{s\in S} \mathrm{div}\boldsymbol{w}(s)}{|S|}$ and $\frac{\sum_{s\in S} \mathrm{curl}\boldsymbol{w}(s)}{|S|}$. These results show clearly the superiority of the adapted div-curl smoothness to recover divergent and rotational motions, but at a double cpu time expense. Besides, compared to a quadratic div-curl smoothing term, the use of a robust penalty improves slightly the accuracy of the results for a modest increase of computation time. It is also

Table 2: Comparative Results for Synthetic Motions

| *Regularization* | (div, curl) | *Mean Square Error* | *Average* div | *Average* curl | *CPU time* |
|---|---|---|---|---|---|
| Robust generic | $(0.2, 0.0)$ | 43.77 | 0.09 | $-0.003$ | 125s |
| Quadratic div-curl | $(0.2, 0.0)$ | 11.86 | 0.1706 | 0.0017 | 275s |
| Robust div-curl | $(0.2, 0.0)$ | **11.18** | **0.1873** | **0.002** | 290s |
| Robust generic | $(0.0, -0.2)$ | 41.91 | 0.04 | $-0.11$ | 135s |
| Quadratic div-curl | $(0.0, -0.2)$ | 15.22 | $-0.0122$ | $-0.1935$ | 239s |
| Robust div-curl | $(0.0, -0.2)$ | **14.90** | $\mathbf{-0.009}$ | **-0.1978** | 246s |
| Robust generic | $(0.2, -0.2)$ | 47.64 | 0.09 | $-0.05$ | 135s |
| Quadratic div-curl | $(0.2, -0.2)$ | 14.32 | 0.1795 | $-0.1731$ | 269s |
| Robust div-curl | $(0.2, -0.2)$ | **12.36** | **0.1820** | **-0.1853** | 275s |

quite informative to compare the different motion fields and div/curl estimates provided by the different approaches. We present in figures 3, 4 and 5 for the three different sequences the motion fields and the corresponding maps of divergence and vorticity estimated with

the robust first-order smoothness and with the adapted div-curl regularization. These

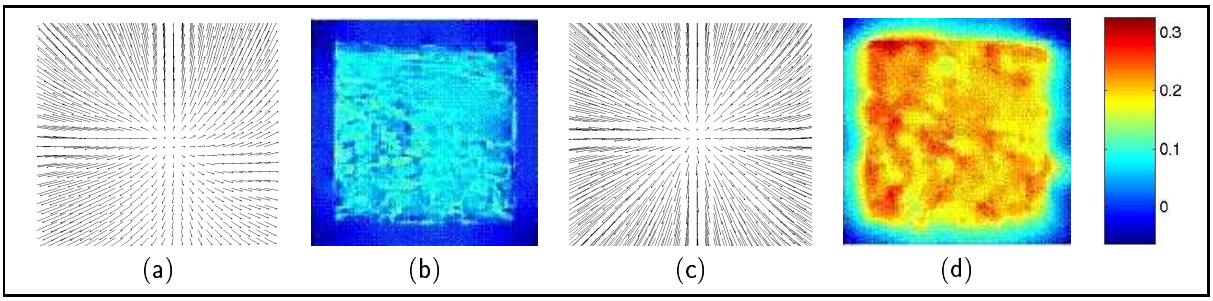


Figure 3: – *Diverging motion – Motion field and corresponding divergence estimated with a robust first-order regularization* (a,b) *and with the proposed div-curl smoothing* (c,d)

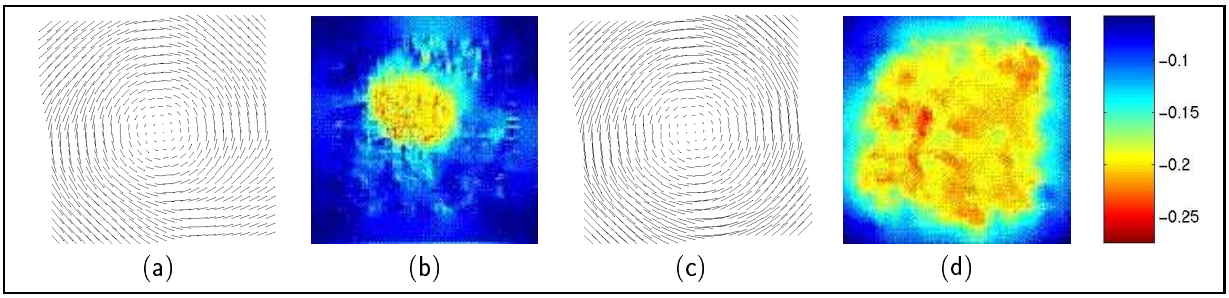


Figure 4: – *Rotational motion – Motion field and corresponding vorticity estimated with a robust first-order regularization* (a,b)*, and with the proposed div-curl smoothing* (c,d)*.*

visualizations confirm the fact that a generic estimator (even including robust functions) can hardly recover the true diverging/rotational motions. The div-curl regularization appears to be far more reliable to estimate such essential components of fluid motion.

To study the behavior of the data-model based on continuity equation, we have consider a fourth synthetic sequence (figure 6). This sequence simulates a diverging motion with div $= 0.2$ accompanied by the corresponding loss of intensity predicted by equation (15). More precisely, according to our model, the intensity of the second image is weighted everywhere by $\exp(-\mathrm{div}(\boldsymbol{w})) = \exp(-0.2) = 0.818$. On this sequence, we have compared the generic technique based on the optical flow constraint with a first-order smoothness, and the complete dedicated approach constituted of a div-curl regularization associated to a data model relying on the continuity equation. The obtained results are shown in Figure 7. As expected, the generic estimator is absolutely not adapted to this type of situations (see Fig. 7 (a) and (b)). The brightness constancy constraint is indeed unable to match corresponding

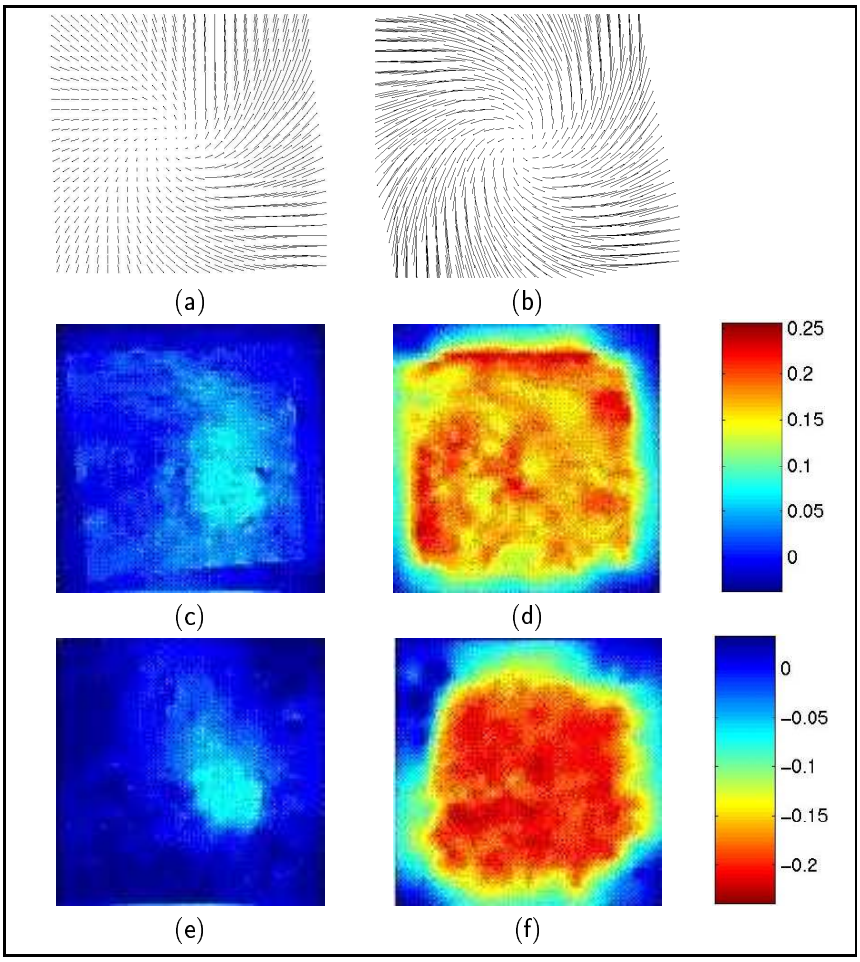


Figure 5: – *Swirling motion – Motion field and corresponding divergence (second line) and vorticity (third line) maps estimated with a robust first-order regularization* (a, c, e)*, and with the proposed div-curl smoothing* (b, d, f)*.*

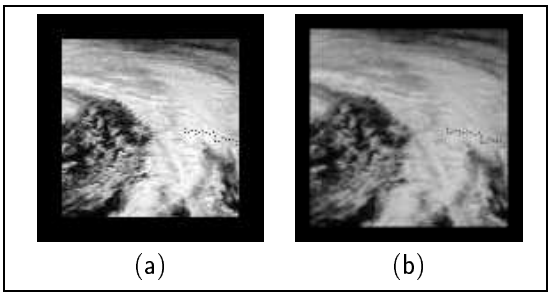


Figure 6: *(a) Original Meteosat image (visible channel); (b) synthetic divergence accompanied by a loss of intensity.*

points. Figure 7 (c) presents the results corresponding to the proposed dedicated model. The average divergence of the two motion fields is respectively div = 0.0943 for the generic estimator and div = 0.2041 for the dedicated estimator. Since this synthetic example was perfectly compliant with the integrated continuity equation, not much should be concluded from this comparison, except that the dedicated model provides consistent estimates in this favorable case. The actual method must be (qualitatively) validated on real sequences.

We now turn to such comparisons on real world meteorological sequences.

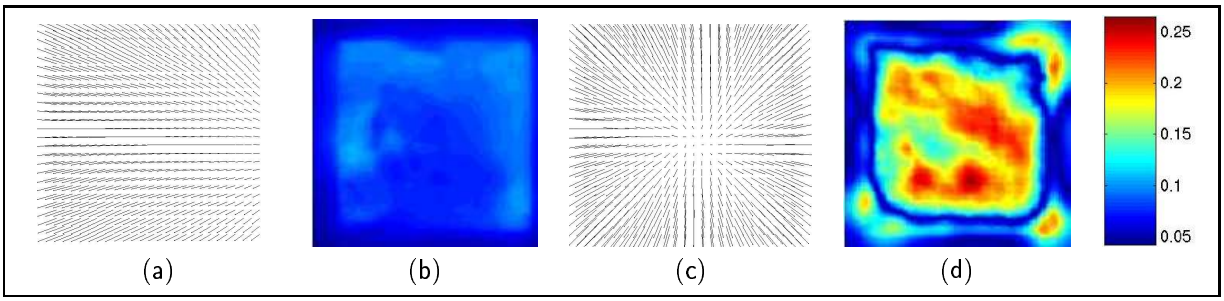


Figure 7: *– Diverging sequence with loss of intensity – Motion field and divergence estimated with a first-order regularization term and the brightness constancy assumption (a,b), and with our div-curl technique associated with a data model based on the continuity equation (c,d).*

## 6.2 Real world sequences

We have chosen to show results on two different kinds of meteorological image sequences. The first one, issued from the infra-red channel of Meteosat (Fig.8a,b), has been shot the $21^{st}$ of January 1998 and shows a large through of low pressure (lower left part of the image)

together with a large cloud structure moving in the upper right part of the image. Figures 8c and 8d show, for two consecutive images of that sequence, the motion fields estimated with the robust generic technique and with the proposed dedicated method. The corresponding vorticity and divergence fields are also presented in figure 9. In the two cases, the flows recovered are physically plausible. Nevertheless, the generic estimator seems to smooth out too much the rotational and the divergence parts of the motion field. With the dedicated model the full extent of the depression swirling motion is recovered and the diverging motion of the upper right structure can be more clearly observed[1]. These observations are also

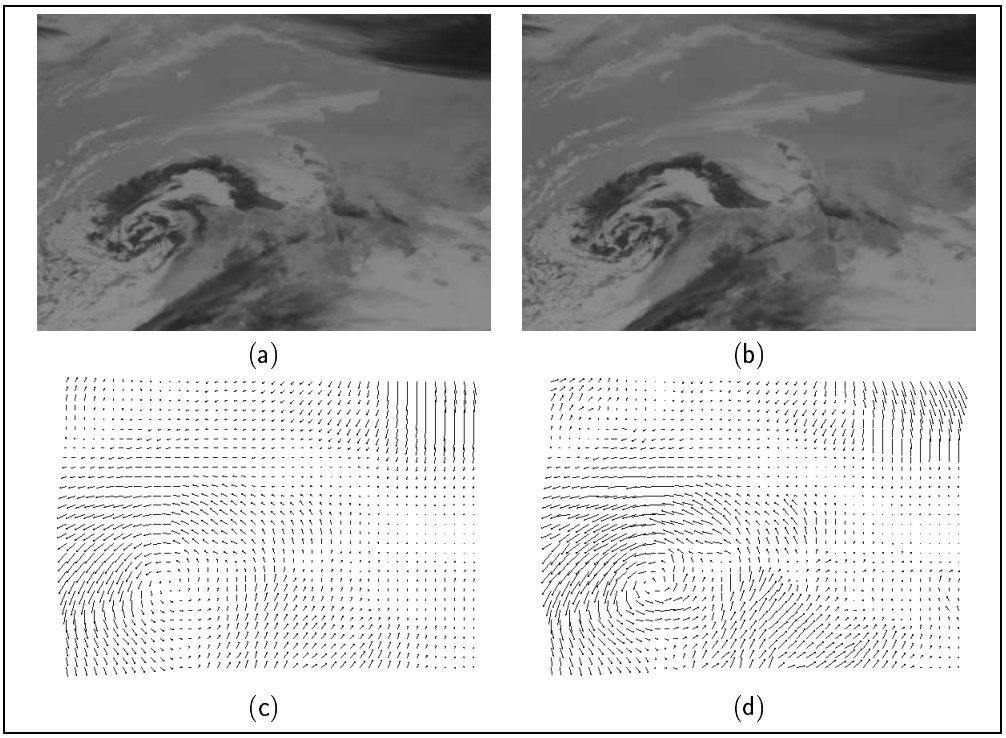


Figure 8: *–Infra-red Meteosat sequence – Two consecutive images (a,b); motion fields estimated with the robust generic technique (c) and with the dedicated method (d)*

supported by the comparison of the associated vorticity and divergence fields (Fig. 9). This comparison shows clearly the ability of the dedicated approach to recover the concentrations of divergence and vorticity (Fig. 9c and 9d). Of course the true value of these quantities are completely unknown, but as shown in a second part of this section, a closer analysis of the

[1]The complete sequences and the results can be played at `http://www.irisa.fr/vista/Themes/Demos/MouvementFluide/fluide.english.html`

results along the complete sequence –which comprises 14 images – demonstrates clearly the superiority of the dedicated approach on this sequence.

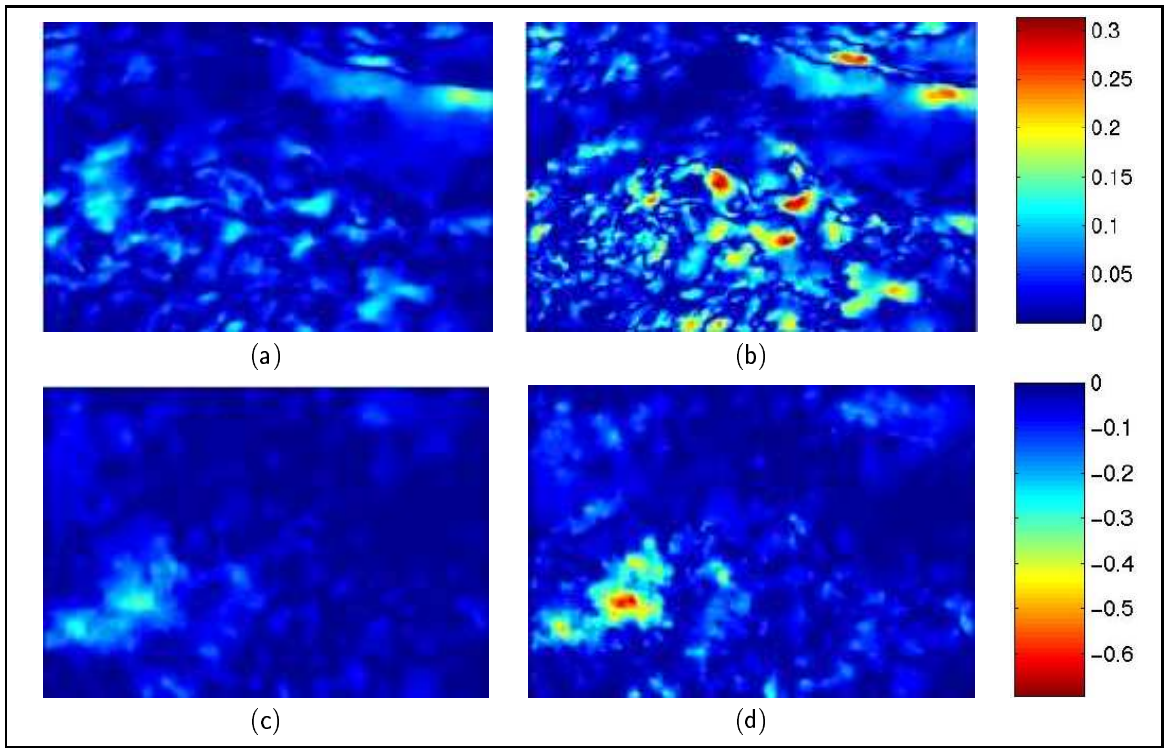


Figure 9: – *Infra-red Meteosat sequence – Divergence (first line) and vorticity (second line) maps estimated with the generic robust technique* (a,c) *and with the dedicated div-curl approach* (b,d).

The second satellite sequence (Fig. 10) is a water vapor image sequence shot the $4^{th}$ of August 1995. This sequence represents a through of low pressure on the left part of the image and a set of active convective cells on the right part. Water-vapor images contain many relevant informations for specialists. But, due to their low photometric contrast, their study is a tough problem. The figure 11 presents the motion fields estimated on 5 consecutive images of the sequence with the generic motion estimator and with the dedicated technique. Let us point out that to ensure a minimum of temporal coherence, the procedure is initialized – for both estimator, at coarsest resolution and grid level – by the dense motion field estimated at the preceding instant. As for the first image couple, the procedure is initialized by a null field.

The motion fields obtained show clearly the differences between the two approaches. The

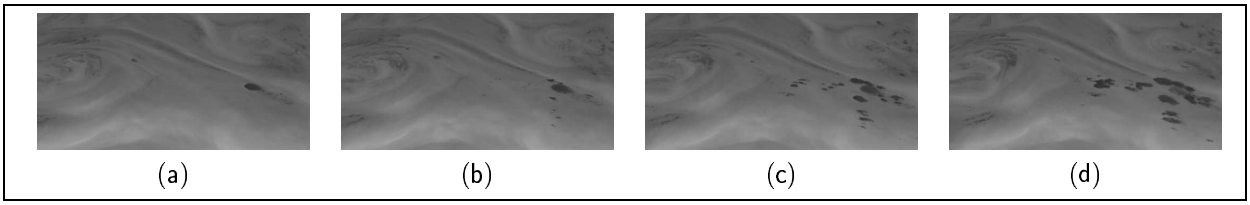


Figure 10: – *Water vapor image sequence – 5 images shot from 10:00 am to 13:00 pm at the rate of one image per hour*

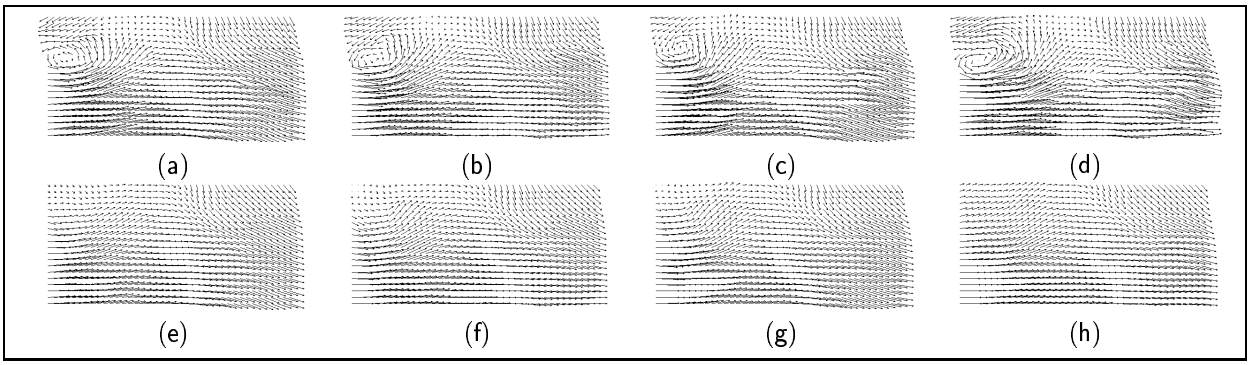


Figure 11: – *Water vapor image sequence – Vector fields estimated with the dedicated div-curl method (*a, b, c, d*) and with the generic robust approach (*e, f, g, h*).*

generic technique smoothes the motion field in such a way that the swirling motion of the depression is completely lost. At the opposite, the dedicated model demonstrates its capacity to recover such motions in low contrast situations. Furthermore, the observation of the consecutive motion fields indicates a certain stability in the motion estimation computed with our model. This characteristic will be confirmed in the next section where we compute the trajectories of some points along the 22 images of the sequence. The vorticity and divergence obtained for the dedicated div-curl estimator are displayed in figure 12.

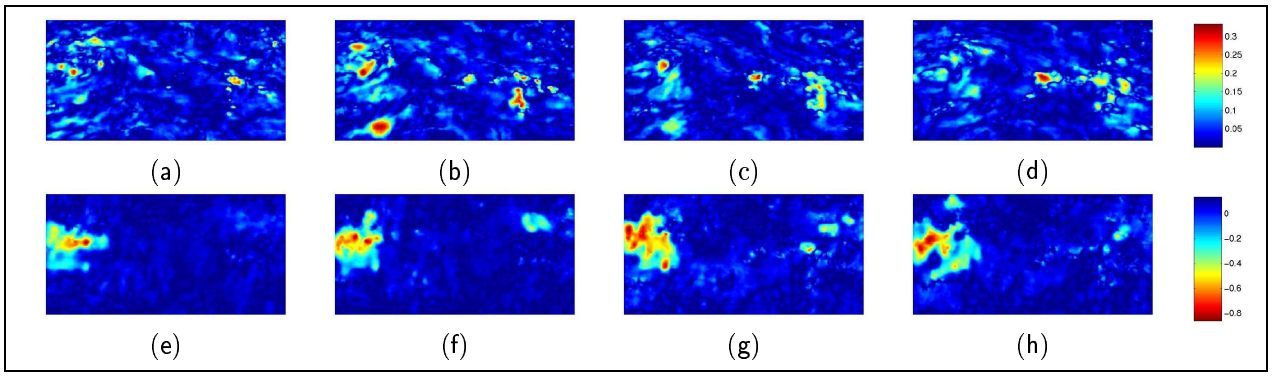


Figure 12: – *Water vapor image sequence – successive maps of divergence* (a,b,c,d) *and vorticity* (e,f,g,h) *estimated with the dedicated estimator*

To assess further the quality of the motion fields recovered over time, we now present an application of trajectory reconstruction. Results on a long time period can thus be visualized to compare qualitatively the proposed dedicated motion estimator to the generic robust one. Besides, to show the quality and the usefulness of the estimated divergence and vorticity fields, we finally present a second application where one tries to detect the areas exhibiting high concentration of divergence or vorticity.

## 6.3 Application I: Trajectory reconstruction

The reconstruction of the trajectories of some elements of fluid through time is a problem of practical interest on its own right. It indeed allows to get so-called Lagrangian drifters which can complement or even replace the use of complicated, expensive, and sparse physical drifters in a number of applications ranging from fish eggs tracking to atmospheric polluant tracking. Apart from this applicative interest, the reconstruction of trajectories provides a unique visualization tool to assess the quality of estimated motion fields. As suggested in [40], this reconstruction is conducted with a Runge-Kutta integration method. Knowing the (dense) motion fields $\boldsymbol{w}(t_0 + n\Delta t) = \{\boldsymbol{w}(\boldsymbol{x}, t_0 + n\Delta t), \boldsymbol{x} \in S\}$, $n = 0, \cdots, N-1$ for a sequence of $N+1$ images, we aim to reconstruct the trajectory $\boldsymbol{x}(t)$ of some point located at $\boldsymbol{x}_0$ in the first image: $\boldsymbol{x}(t_0) = \boldsymbol{x}_0$. Assuming that the position function is differentiable,

the velocity is given by

$$\frac{d\boldsymbol{x}(t)}{dt} \simeq \frac{\boldsymbol{w}(\boldsymbol{x}(t),t)}{\Delta t}.$$

We thus have to conduct numerical integration of an O.D.E. with initial condition. *Runge-Kutta* methods are standard numerical techniques to solve this problem. They consist to approximate

$$\underbrace{\boldsymbol{x}(t_0+(n+1)\Delta t)}_{\triangleq \boldsymbol{x}_{n+1}} - \underbrace{\boldsymbol{x}(t_0+n\Delta t)}_{\triangleq \boldsymbol{x}_n} = \int_{t_0+n\Delta t}^{t_0+(n+1)\Delta t} \boldsymbol{x}'(t)dt = \int_{t_0+n\Delta t}^{t_0+(n+1)\Delta t} \frac{\boldsymbol{w}(\boldsymbol{x}(t),t)}{\Delta t}dt. \quad (29)$$

A fourth-order approximation gives:

$$\boldsymbol{x}_{n+1} = \boldsymbol{x}_n + \frac{1}{6}(\boldsymbol{w}_n^{(1)} + 2\boldsymbol{w}_n^{(2)} + 2\boldsymbol{w}_n^{(3)} + \boldsymbol{w}_n^{(4)}) \quad (30)$$

where:

$$\begin{cases} \boldsymbol{w}_n^{(1)} &= \boldsymbol{w}(\boldsymbol{x}_n, t_0+n\Delta t) \\ \boldsymbol{w}_n^{(2)} &= \boldsymbol{w}(\boldsymbol{x}_n + \frac{\boldsymbol{w}_n^{(1)}}{2}, t_0+n\Delta t+\frac{\Delta t}{2}) \\ \boldsymbol{w}_n^{(3)} &= \boldsymbol{w}(\boldsymbol{x}_n + \frac{\boldsymbol{w}_n^{(2)}}{2}, t_0+n\Delta t+\frac{\Delta t}{2}) \\ \boldsymbol{w}_n^{(4)} &= \boldsymbol{w}(\boldsymbol{x}_n + \boldsymbol{w}_n^{(3)}, t_0+n\Delta t+\Delta t). \end{cases}$$

In our case, $\boldsymbol{w}$ has to be interpolated in time and space from the discrete motion fields, using bilinear interpolation.

We present results obtained for the complete sequences shown previously. The first one is a 14 infra-red image sequence shot the $21^{th}$ of January 1998. The second sequence is composed of 22 water vapor image shot the $4^{th}$ August 1995. Reconstructed trajectories based on the dedicated div-curl estimator are shown in Fig. 14 both for a regular grid of points and for a selection of some points. Initial positions from which trajectories are reconstructed are shown, superimposed to the first image of the sequence, in figure 13.

The recovered trajectories (Fig. 14) seem physically plausible and compliant with the actual motion – or at least with the idea provided by visual inspection[2]. Trajectories computed from initial points shown in Fig. 13 are *superimposed to the last image of the sequence* in Fig. 14. The quality of these trajectories demonstrates the relevance of the instantaneous motion fields estimated by our method as well as their temporal stability within a long time period despite the absence of explicit temporal link within the estimator (apart from the use of previous estimate as an initial guess).

The corresponding results obtained with the generic robust estimator are shown on figure 15. The location of original points and the time period are the same than before. It

[2]The complete sequences and the reconstructed trajectories may be seen at `http://www.irisa.fr/vista/Themes/Demos/MouvementFluide/fluide.english.html`

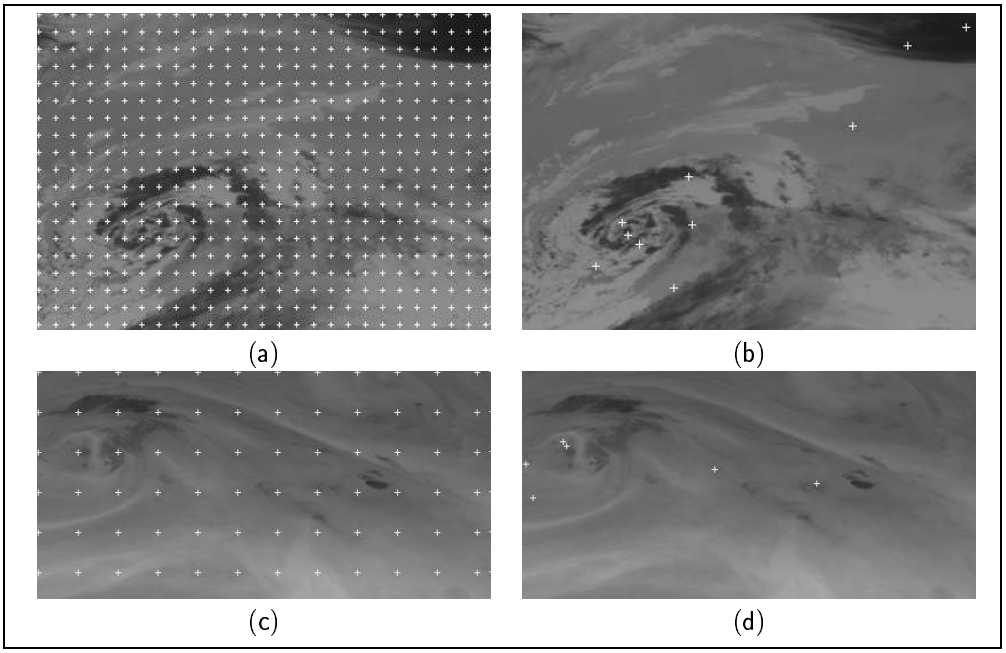


Figure 13: *Initial points from which trajectories are reconstructed. For the infra-red sequence,*(a) *is a regular grid of starting points, and* (b) *is a selection of ten given points; for the water-vapor sequence,* (c) *is a regular grid of starting points and* (d) *is a selection of six given starting points.*

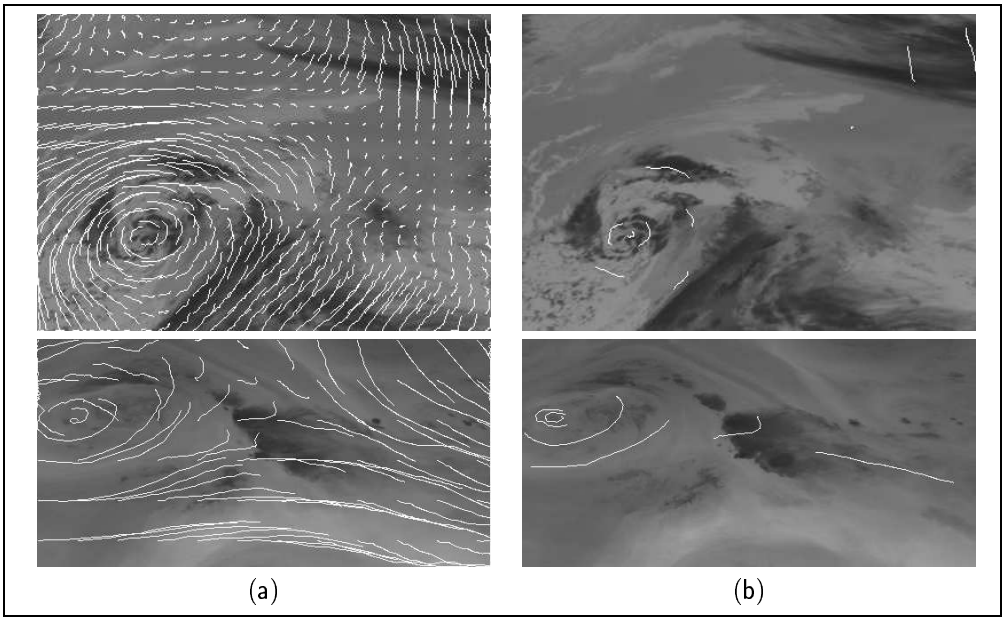


Figure 14: *Reconstructed trajectory obtained from velocity fields estimated with the dedicated fluid motion estimation technique;* (a) *for a regular grid of initial points;* (b) *for a selection of starting points, and superimposed on the last image of the sequence (see Fig 13 for location of starting points in the first image)*

appears that the generic robust estimator based on robust first-order regularization leads to much smoother trajectories which are obviously less compliant with the real apparent motion. In the case of the water-vapor sequence, the generic technique does not detect the depression in the left part of the image. In that example, the rather low level of photometric information makes the motion (and therefore trajectories) estimation driven a lot by the first-order regularization. This prevents from recovering properly the complicated motion within the low pressure area. Nevertheless, even in the infra-red sequence where the photometric information is much reacher and more reliable, the first-order regularization still attenuates the estimates in the low pressure area and in the divergent one. Some valuable informations are thus completely smoothed out.

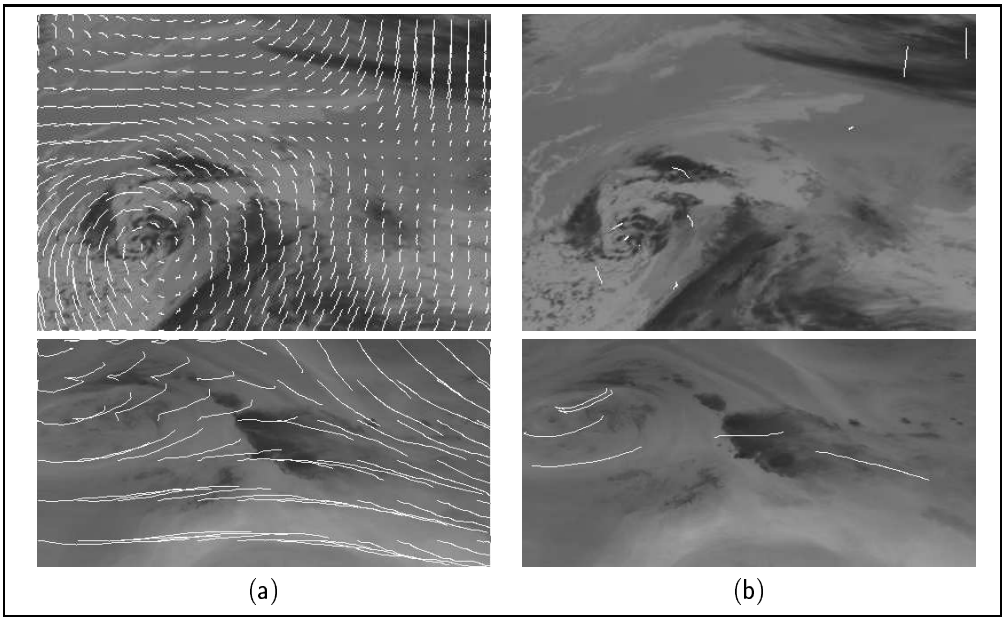


Figure 15: *Reconstructed trajectory obtained from velocity fields estimated with the generic robust technique;* (a) *for a regular grid of initial points;* (b) *for a selection of starting points, and superimposed on the last image of the sequence (see Fig 13 for location of starting points in the first image)*

## 6.4 Application II: Extraction of significant areas of vorticity and divergence

From an appropriate motion estimation, it might be extremely interesting to extract the areas of significant divergence and vorticity. As a matter of fact, these areas retain structures that are of key importance for understanding as well as describing fluid flows [18, 33]. The

extraction of these structures can be cast as the estimation of binary maps ($\ell_{\text{div}}$ and $\ell_{\text{curl}}$), indicating the presence/absence of diverging motion and of rotational motion. To recover these two label fields $\ell_{\text{div}} = \{\ell_{\text{div}}(s), s \in S\}$ and $\ell_{\text{curl}} = \{\ell_{\text{curl}}(s), s \in S\}$, we have adopted a standard energy-based model in which the unknown labels interact on a local basis. In the following, we only introduce the model used for detection of diverging areas. This model is extended straightforwardly to the detection of concentrations of vorticity. The estimation of $\ell_{\text{div}}$ is posed as the research of the minimizer of an energy function:

$$U(\ell_{\text{div}}) = \sum_{s \in S} V_1(\xi_s, \ell_{\text{div}}(s)) + \beta \sum_{<s,r> \in C} V_2(\ell_{\text{div}}(s), \ell_{\text{div}}(r)) \tag{31}$$

where $\xi$ denotes the estimate of divergence of vector field $\boldsymbol{w}$. The positive parameter $\beta$ controls the relative importance of the contextual energy term. We choose potential $V_1$ as:

$$V_1(\xi_s, \ell_{\text{div}}(s)) = \begin{cases} \frac{\xi_s}{\xi_s + \mu} & \text{if } \ell_{\text{div}}(s) = 0 \\ 1 - \frac{\xi_s}{\xi_s + \mu} & \text{if } \ell_{\text{div}}(s) = 1, \end{cases} \tag{32}$$

where $\mu$ is a given threshold. Potential $V_1$ has been chosen heuristically such that if $\xi(s) < \mu$ (resp. $\xi(s) > \mu$), the minimizer of $V_1(\xi(s), \ell_{\text{div}}(s))$ is $\ell_{\text{div}}(s) = 0$ (resp. $\ell_{\text{div}}(s) = 1$). Figure 16 shows a plot of functions $V_1(\xi(s), 0)$ and $V_1(\xi(s), 1)$.

To enforce compact areas the *a priori* term is defined as:

$$V_2(\ell_{\text{div}}(s), \ell_{\text{div}}(r)) = 2\delta(\ell_{\text{div}}(s) - \ell_{\text{div}}(r)) - 1. \tag{33}$$

The global optimization of $U(\ell_{\text{div}})$ is conducted with the ICM deterministic minimization method [6]. It is initialized by the minimizer of the first term only (i.e., the binary map associated to the thresholding of $\xi$ at level $\mu$).

Figures 17 (resp.18) presents detection results for a pair of images of the water vapor sequence (resp. the infra-red sequence).

We present also results obtained on another infra-red Meteosat sequence showing some convective clouds whose upward motion results in a divergent motion in the 2D image plane. The extraction of such structures is of actual importance for weather forecasting since they are responsible of sudden and violent meteorological events (such as showers, storms,...). In these three sequences, the estimated detection maps seem to capture consistently the main areas of vorticity and divergence, whereas the application of the same extraction technique on the fields provided by the generic model does not provide sensible results (either nothing significant or a much too noisy detection map). The divergence and vorticity estimated by the way of the proposed dedicated motion estimator can thus constitute valuable inputs for extracting simply kinematic features of interest in number of applications. This is a new evidence supporting the relevance of the proposed dedicated model for fluid motion analysis.

# 7 Conclusion

In this paper, we have presented a new method for estimating fluid flows from image sequences. This method is an extension of the energy-based generic robust models where an

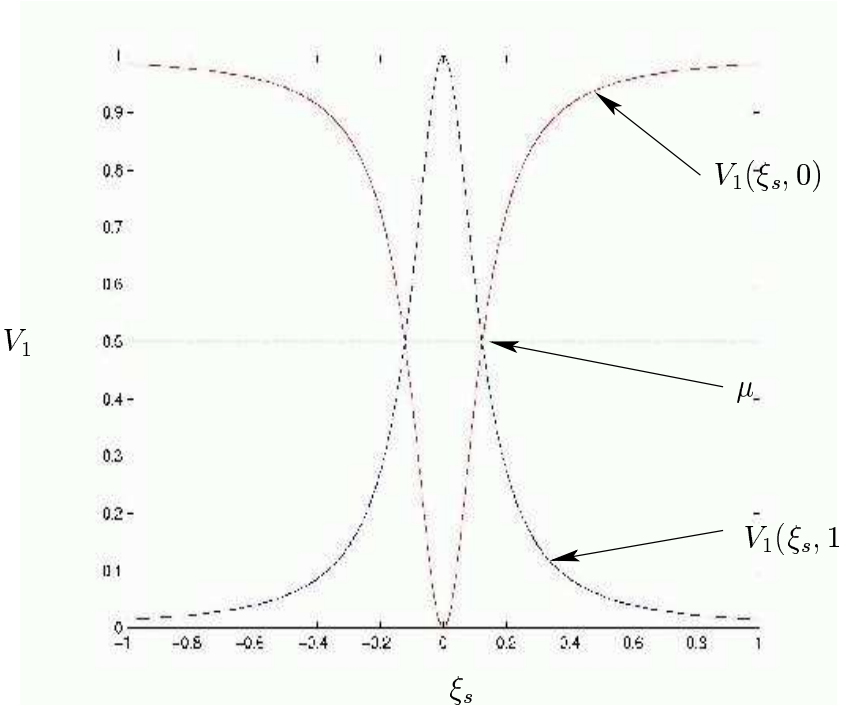


Figure 16: *Data model potential function* $V_1(\xi_s, \ell_{div}(s))$, $\mu = 0.15$

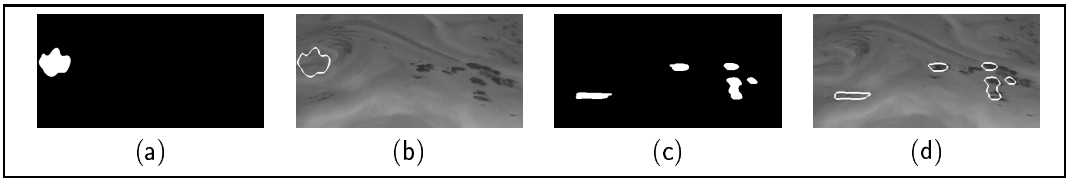


Figure 17: – *Water-vapor sequence – Extraction of pertinent structures of the flow;*(a,b) *vorticity areas;* (c,d) *diverging areas.*

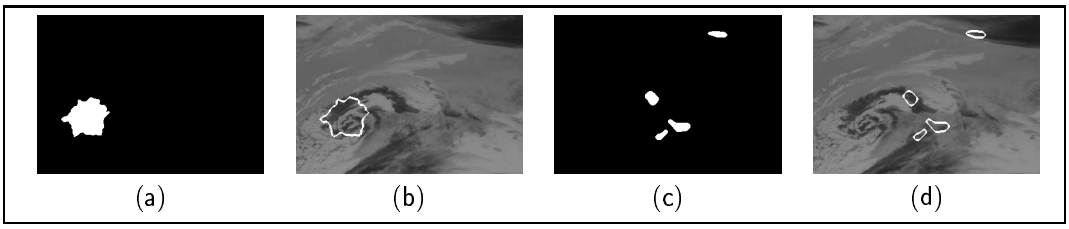


Figure 18: – *Infra-red sequence – Extraction of pertinent structures of the flow;(*a,b*) vorticity areas; (*c,d*) diverging areas.*

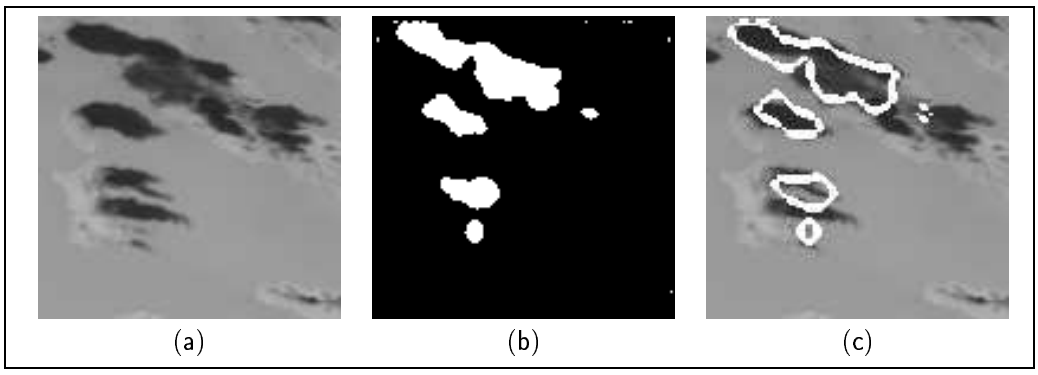


Figure 19: *(*a*) Convective clouds in infra-red images. (*b,c*): extraction of significant divergent areas.*

objective function, constituted of data-model term in association with a smoothness prior, is to be minimized. Both terms have been specifically designed to suit image sequences representing fluid phenomena evolving in time.

The data-model arises from the mass conservation of fluid flow known as *continuity equation*. An integration of this equation has allowed us to define a new data-model that can be embedded within an incremental minimization scheme. The smoothing part of the model is based on the idea of div-curl regularization. We have shown that the overall model may be implemented as the minimization of a discrete energy function relying on a non-symmetric discretization of the divergence and rotational operators. The optimization of the complete model is set in a multiresolution/multigrid optimization framework for improved quality and speed.

This new technique has been validated both on synthetic and real sequences, and with two kinds of Meteosat images (infra-red and water vapor channels). On this kind of data the proposed dedicated motion estimation model has demonstrated its superiority on a generic robust technique. It has especially proved its usefulness in recovering the components of the motion that are of critical importance for analyzing, understanding (and predicting) fluid phenomena. The temporal stability and the accuracy of the estimated motion fields have been also assessed by the way of trajectory reconstructions over long time sequences.

As estimating motion in fluid sequences is an important prerequisite in a number of domains, we believe that the dedicated model introduced in this paper provides a useful tool. Although the computational cost is large, it is already acceptable for a number of target applications (especially meteorological and oceanographic applications). Nevertheless, if the method was to be used in an experimental context with higher time constraints, such as some applications in experimental fluid mechanics, the integration of proposed algorithms in fast architectures can reasonably be envisaged. Apart from the two examples of utilization of estimated motion fields (computation of numerical Lagrangian drifters, and extraction of vorticity/divergent concentrations), other high level task, including the detection, the recognition, and the tracking of entities of interest (e.g., depressions or low-cloud in meteorology, pathological blood vortices in heart angiography) could hopefully rely on obtained vectors fields.

# References

[1] A. Amini. A scalar function formulation for optical flow. In *Proc. Europ. Conf. Computer Vision*, pages 125–131, 1994.

[2] G. Aubert, R. Deriche, and P. Kornprobst. Computing optical flow via variational techniques. *SIAM Journal on Applied Mathematics*, 60(1):156–182, 1999.

[3] L. Bannehr, M. Rohn, and G. Warnecke. A functionnal analytic method to derive displacement vector fields from satellite image sequences. *Int. Journ. of Remote Sensing*, 17(2):383–392, 1996.

[4] D. Béréziat, I. Herlin, and L. Younes. A generalized optical flow constraint and its physical interpretation. In *Proc. Conf. Comp. Vision Pattern Rec.*, volume 2, pages 487–492, Hilton Head Island, South Carolina, USA, 2000.

[5] J. Bergen, P. Anandan, K. Hanna, and R. Hingorani. Hierarchical model-based motion estimation. In G. Sandini, editor, *Proc. Europ. Conf. Computer Vision*, volume 558 of *LNCS*, pages 237–252. Springer-Verlag, 1992.

[6] J. Besag. On the statistical analysis of dirty pictures. *J. Royal Statist. Soc.*, 48 B(3):259–302, 1986.

[7] M. Black and P. Anandan. The robust estimation of multiple motions: Parametric and piecewise-smooth flow fields. *Computer Vision and Image Understanding*, 63(1):75–104, 1996.

[8] M. Black and A. Rangarajan. On the unification of line processes, outlier rejection, and robust statistics with applications in early vision. *Int. J. Computer Vision*, 19(1):75–104, 1996.

[9] P.J. Burt. The pyramid as a structure for efficient computation. In A. Rozenfeld, editor, *Multiresolution Image Processing and Analysis*, pages 6–35. Springer-Verlag, 1984.

[10] G. Christensen, R. Rabbit, and M.I. Miller. Deformable templates using large deformation kinematics. *IEEE Trans. Image Processing*, 5(10):1435–1447, 1996.

[11] I. Cohen and I. Herlin. Non uniform multiresolution method for optical flow and phase portrait models: Environmental applications. *Int. J. Computer Vision*, 33(1):29–49, 1999.

[12] A. Delanay and Y. Bresler. Globally convergent edge-preserving regularized reconstruction: an application to limited-angle tomography. *IEEE Trans. Image Processing*, 7(2):204–221, 1998.

[13] W. Enkelmann. Investigation of multigrid algorithms for the estimation of optical flow fields in image sequences. *Comp. Vision Graph. and Image Proces.*, 43:150–177, 1988.

[14] J.M. Fitzpatrick. A method for calculating velocity in time dependent images based on the continuity equation. In *Proc. Conf. Comp. Vision Pattern Rec.*, pages 78–81, San Francisco, USA, 1985.

[15] J.M. Fitzpatrick. The existence of geometrical density-image transformations corresponding to object motion. *Comput. Vision, Graphics, Image Proc.*, 44(2):155–174, 1988.

[16] J.M. Fitzpatrick and C.A. Pederson. A method for calculating fluid flow in time dependant density images. In *Electronic Imaging*, volume 1, pages 347–352, 1988. Institute for Graphic Communication.

[17] R.M. Ford. Critical point detection in fluid flow images using dynamical system properties. *Pattern Recognition*, 30(12):1991–2000, 1997.

[18] R.M. Ford and R. Strickland. Representing and visualizing fluid flow images and velocimetry data by nonlinear dynamical systems. *Graph. Mod. Image Proc.*, 57(6):462–482, 1995.

[19] R.M. Ford, R. Strickland, and B. Thomas. Image models for 2-d flow visualization and compression. *Graph. Mod. Image Proc.*, 56(1):75–93, 1994.

[20] D. Geman and G. Reynolds. Constrained restoration and the recovery of discontinuities. *IEEE Trans. Pattern Anal. Machine Intell.*, 14(3):367–383, 1992.

[21] S. Gupta and J. Prince. Stochastic models for div-curl optical flow methods. Technical Report Jhu/Ece 95-18, John Hopkins Univ., Dpt Electrical and Comp. Eng., May 1995.

[22] S. Gupta and J. Prince. Stochastic models for div-curl optical flow methods. *Signal Proc. Letters*, 3(2):32–34, 1996.

[23] P. Hellier, C. Barillot, E. Mémin, and P. Pérez. An energy-based framework for dense 3D registration of volumetric brain image. In *Proc. Conf. Comp. Vision Pattern Rec.*, Hilton Head Island, South Carolina, USA, June 2000.

[24] P. Holland and R. Welsch. Robust regression using iteratively reweighted least-squares. *Commun. Statis.-Theor. Meth.*, A6(9):813–827, 1977.

[25] B. Horn and B. Schunck. Determining optical flow. *Artificial Intelligence*, 17:185–203, 1981.

[26] X. Ju, M.J. Black, and A.D. Jepson. Skin and bones: Multi-layer, locally affine, optical flow and regularization with transparency. In *Proc. Conf. Comp. Vision Pattern Rec.*, pages 307–314, 1996.

[27] P. Kornprobst, R. Deriche, and G. Aubert. mage sequence analysis via partial differential equations. *Journal of Mathematical Imaging and Vision*, 11(1):5–26, September 1999.

[28] S. Lai and B. Vemuri. Reliable and efficient computation of optical flow. *Int. Journ of Comp. Vision*, 29(2):87–105, 1998.

[29] R. Larsen, K. Conradsen, and B.K. Ersboll. Estimation of dense image flow fields in fluids. *IEEE trans. on Geoscience and Remote sensing*, 36(1):256–264, 1998.

[30] M. Maurizot, P. Bouthemy, and B. Delyon. 2D fluid motion analysis from a single image. In *IEEE Int. Conf. on Computer Vision and Pattern Recognition*, pages 184–189, Santa Barbara, 1998.

[31] E. Mémin and P. Pérez. Dense estimation and object-based segmentation of the optical flow with robust techniques. *IEEE Trans. Image Processing*, 7(5):703–719, 1998.

[32] E. Mémin and P. Pérez. A multigrid approach for hierarchical motion estimation. In *Proc. Int. Conf. Computer Vision*, pages 933–938, Bombay, India, 1998.

[33] E. Mémin and P. Pérez. Fluid motion recovery by coupling dense and parametric motion fields. In *Proc. Int. Conf. Computer Vision*, volume 3, pages 732–736, Corfou, Greece, 1999.

[34] E. Mémin and T. Risset. VLSI design methodology for edge-preserving image reconstruction. *Real-Time Imaging*, accepted for publication.

[35] P. Nesi. Variational approach to optical flow estimation managing discontinuities. *Image and Vision Computing*, 11(7):419–439, 1993.

[36] H. Nogawa, Y. Nakajima, and Y. Sato. Acquisition of symbolic description from flow fields: a new approach based on a fluid model. *IEEE Trans. Pattern Anal. Machine Intell.*, 19(1):58–63, 1997.

[37] A. Nomura, H. Miike, and K. Koga. Field theory approach for determining optical flow. *Pattern Recognition Letters*, 12(3):183–190, 1991.

[38] A. Ottenbacher, M. Tomasini, K. Holmund, and J. Schmetz. Low-level cloud motion winds from Meteosat high-resolution visible imagery. *Weather and Forecasting*, 12(1):175–184, 1997.

[39] C. Papin, P. Bouthemy, E. Mémin, and G. Rochard. Tracking and characterization of highly deformable cloud structures. In *Proc. Europ. Conf. Computer Vision*, Dublin, 2000.

[40] D. Ramsden and G. Holloway. Time-stepping Lagrangian particles in two dimensional Eulerian flow fields. *J. Comput. Phys.*, 95:101–116, 1991.

[41] C. Schnorr, R. Sprengel, and B. Neumann. A variational approach to the design of early vision algorithms. *computing Suppl.*, pages 149–165, 1996.

[42] B.G. Schunk. The motion constraint equation for optical flow. In *Proc. Int. Conf. Pattern Recognition*, pages 20–22, Montreal, 1984.

[43] J.J. Simpson and J.I. Gobat. Robust velocity estimates, stream functions, and simulated Lagrangian drifters from sequential spacecraft data. *IEEE trans. on Geosciences and Remote sensing*, 32(3):479–492, 1994.

[44] S.M. Song and R.M. Leahy. Computation of 3D velocity fields from 3D cine and CT images of human heart. *IEEE trans. on medical imaging*, 10(3):295–306, 1991.

[45] D. Suter. Motion estimation and vector splines. In *Proc. Conf. Comp. Vision Pattern Rec.*, pages 939–942, Seattle, USA, June 1994.

[46] J. Wallace and J. Foss. The measurement of vorticity in turbulent flows. *Annu. Rev. Fluid Mech.*, 27:469–514, 1995.

[47] R. Wildes, M. Amabile, A.M. Lanzillotto, and T.S. Leu. Physically based fluid flow recovery from image sequences. In *Proc. Conf. Comp. Vision Pattern Rec.*, pages 969–975, 1997.

## Relationship between div-curl and first-order regularization

By using the *Euler-Lagrange* condition of minimality, the equivalence between a standard first-order smoothness regularization, and a div-curl regularization with same weights for div and curl penalties can be readily demonstrated. Recall that Euler-Lagrange equation constitutes a necessary conditions for the minimization with respect to function $g(x,y)$ of a funtional

$$\int_{\mathcal{S}} \mathcal{F}(g, g_x, g_y, x, y) d\boldsymbol{s}.$$

It reads:

$$\frac{\partial \mathcal{F}}{\partial g} - \frac{\partial}{\partial x}\frac{\partial \mathcal{F}}{\partial g_x} - \frac{\partial}{\partial y}\frac{\partial \mathcal{F}}{\partial g_y} = 0$$

Assuming a first-order regularization term

$$H_2(\boldsymbol{w}) = \alpha \int_{\mathcal{S}} (\|\boldsymbol{\nabla} u(s)\|^2 + \|\boldsymbol{\nabla} v(s)\|^2) d\boldsymbol{s},$$

This condition amounts the following coupled PDEs:

$$\left\{ \begin{array}{rcl} -2\alpha u_{xx} - 2\alpha u_{yy} & = & 0 \\ -2\alpha v_{xx} - 2\alpha v_{yy} & = & 0. \end{array} \right. \tag{34}$$

Now, considering a div-curl regularization

$$H_2(\boldsymbol{w}) = \int_{\mathcal{S}} \Big( \alpha \ \mathrm{div}^2 \boldsymbol{w}(s) + \beta \ \mathrm{curl}^2 \boldsymbol{w}(s) \Big) d\boldsymbol{s}, \tag{35}$$

minimality conditions become:

$$\left\{ \begin{array}{rcl} -2\alpha u_{xx} - 2\beta u_{yy} - 2(\alpha - \beta) v_{xy} & = & 0 \\ -2\beta v_{xx} - 2\alpha v_{yy} - 2(\alpha - \beta) u_{xy} & = & 0. \end{array} \right. \tag{36}$$

Where $\alpha = \beta$, these equations are the same as (34)

Unité de recherche INRIA Lorraine, Technopôle de Nancy-Brabois, Campus scientifique,
615 rue du Jardin Botanique, BP 101, 54600 VILLERS LÈS NANCY
Unité de recherche INRIA Rennes, Irisa, Campus universitaire de Beaulieu, 35042 RENNES Cedex
Unité de recherche INRIA Rhône-Alpes, 655, avenue de l'Europe, 38330 MONTBONNOT ST MARTIN
Unité de recherche INRIA Rocquencourt, Domaine de Voluceau, Rocquencourt, BP 105, 78153 LE CHESNAY Cedex
Unité de recherche INRIA Sophia-Antipolis, 2004 route des Lucioles, BP 93, 06902 SOPHIA-ANTIPOLIS Cedex

Éditeur
INRIA, Domaine de Voluceau, Rocquencourt, BP 105, 78153 LE CHESNAY Cedex (France)
http://www.inria.fr
ISSN 0249-6399